STEADY-STATE MOTION OF A MODE-III CRACK ON IMPERFECT INTERFACES

by GENNADY S. MISHURIS

(*Department of Mathematics, Rzeszów University of Technology, Poland*)

NATASHA V. MOVCHAN *and* ALEXANDER B. MOVCHAN

(*Department of Mathematical Sciences, University of Liverpool, Liverpool* L69 3BX)

[Received 29 November 2005. Revise 1 June 2006]

Summary

The aim of the present paper is to analyse the behaviour of the stress and displacement fields in the vicinity of the tip of a crack moving along a bi-material interface. For simplicity, we consider a straight interface of infinite extent. We assume that the two phases are separated by a thin layer which is either 'soft' or 'stiff' compared to the other two phases. We derive the transmission conditions which take into account the material properties of the layer and model the way the load is transferred across the layer from one phase to the other. We assume that the point of interchange in the boundary/transmission conditions coincides with the crack tip that moves along the interface boundary with a constant speed. We develop an integral equation formulation and derive asymptotic formulae for the out-of-plane displacement and the Mode-III stress intensity factor associated with such a motion of the crack inside the interphase layer. The theoretical results are illustrated by numerical examples.

1. Introduction

In recent years there has been substantial interest in static models of elasticity and heat transfer in heterogeneous materials, where interface surfaces are modelled by transmission conditions involving jumps of displacements and/or components of tractions. Examples include rigid inclusions, adhesive joints, inertial and frictional interfaces.

A model of a two-phase composite with an interfacial surface of resistance between the phases was considered by Lipton and Vernescu (**1**) who introduced new variational principles and derived the bounds describing the effective conductivity tensor for such a composite. Asymptotic models of dilute composites with imperfectly bonded inclusions were studied in (**2**). Benveniste and Chen (**3**) considered the Saint-Venant torsion of cylindrical composite bars containing imperfect interfaces. A related study involving asymptotic analysis of fields in thin beams with imperfect interfaces has been done in (**4**). Hashin (**5**) has developed a method for evaluation of the effective elastic moduli of a unidirectional coated fibre composite, with imperfect interface conditions modelling the effect of a thin soft elastic coating. Imperfect transmission conditions for a thin weakly compressible interface have been studied by Mishuris (**6**). The integral equations describing the transmission conditions for rigid inclusions have been derived in (**7**, **8**). A mathematical model for a fibre with a frictional interface has been proposed and analysed in (**9**). Static models of interphases and analysis of stress singularities in linear fracture mechanics were discussed by Atkinson (**10**).

Q. Jl Mech. Appl. Math, Vol. 59. No. 4
Advance Access publication 12 October 2006. doi:10.1093/qjmam/hbl013

Static problems of elasticity and heat transfer in multi-phase composites containing cracks on soft imperfectly bonded bi-material interfaces have been studied in (**11**, **12**). Static Mode-III cracks on stiff interfaces have been considered by Mishuris (**13**).

In the present paper we consider a Mode-III crack moving along a bi-material interface. We assume that the two phases are separated by a thin layer which is either 'soft' or 'stiff' compared to the other two phases. We derive the transmission conditions that take into account the material properties of the layer and the behaviour of the mechanical fields inside it, and give their classifications. The corresponding model problems for a crack moving along an imperfect interface, which replaces the thin layer, are solved using integral transforms. The resulting functional equations are reduced to integral equations with fixed point singularities. We study the uniqueness of solutions of these equations and then solve them numerically. We also analyse the behaviour of the physical fields near the crack tip for stiff and soft interfaces. The results are compared with those for the case of a perfectly bonded interface (**14**). Finally, we look at the delamination crack propagating along a stiff interface. We present several numerical examples which illustrate our results in connection with applications to fracture mechanics.

The paper is organized as follows. The classification of imperfect interfaces and description of transmission conditions are given in section 2. Formulations of mathematical models and the corresponding integral representations of solutions are discussed in sections 3 and 4. Section 5 includes reduction of the model problems to singular integral equations and asymptotic analysis of their solutions. We pay particular attention to the novel asymptotic representations of solutions of model problems and their derivatives near the tip of the moving crack. Finally, section 6 presents numerical simulations and concluding remarks.

2. Classification of interfaces. Transmission conditions

In this paper we consider a Mode-III crack propagating along an interface separating two homogeneous isotropic materials. Before giving the integral equation formulation modelling such a crack, we would like to clarify the notion of imperfect interfaces and show the difference between such interfaces and surfaces of ideal contact.

Assume that a bounded domain Ω of diameter L (see Fig. 1) consists of two parts Ω_+ and Ω_-, separated by a thin layer Π_ε of width $h = \varepsilon h_0$, with ε being a small positive non-dimensional parameter. The domain is subjected to an out-of-plane shear loading; the shear moduli of the materials occupying $\Omega_\pm$ are denoted by $\mu_\pm$. The shear modulus μ of the interphase layer can be either small, similar or large compared to the moduli of the surrounding materials, and this will be essential for the classification of imperfect interfaces.

The displacement functions $u^\pm$ and u in $\Omega_\pm$ and Π_ε satisfy the equations of motion,

$$\mu \Delta u = \rho \ddot{u} \quad \text{in } \Pi_\varepsilon, \quad \mu_\pm \Delta u^\pm = \rho_\pm \ddot{u}^\pm \quad \text{in } \Omega_\pm. \tag{2.1}$$

These equations are supplied with conditions of ideal contact on the boundaries of Π_ε,

$$u^\pm = u, \quad \mu_\pm \frac{\partial u^\pm}{\partial n} = \mu \frac{\partial u}{\partial n} \quad \text{on } \Gamma_\pm, \tag{2.2}$$

where $\Gamma_\pm$ is the boundary between $\Omega_\pm$ and Π_ε, and $\mathbf{n}$ is a unit vector normal to $\Gamma_\pm$.

We consider the case when the wave speed $v = \sqrt{\mu/\rho}$ characterizing the interphase layer Π_ε is either comparable with or larger than the wave speeds $v_\pm = \sqrt{\mu_\pm/\rho_\pm}$ in the domains $\Omega_\pm$.

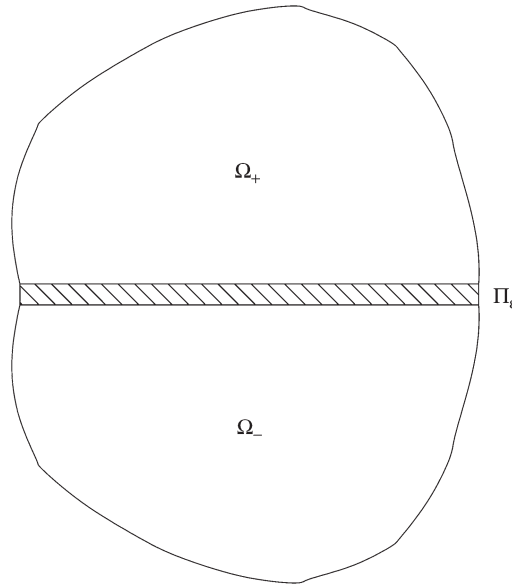

Fig. 1 Composite structure with a thin interphase

2.1 *An outline*

We deal with the interfaces that correspond to the following classes of transmission conditions along the straight line $y = 0$.

1. *Ideal contact interfaces* involve continuity of the displacement and tractions, $u^+(x, 0+, t) = u^-(x, 0-, t)$ and $\mu_+(\partial u^+/\partial y)(x, 0+, t) - \mu_-(\partial u^-/\partial y)(x, 0-, t) = 0$. This is implemented for thin interfacial layers whose elastic constants are of the same order of magnitude as the elastic constants of the ambient media (**15**); $u^\pm$ represent the leading terms of the displacement fields above and below the interface.
2. *Imperfect weak interfaces* assume continuity of tractions and allow for the discontinuity of the displacement; the corresponding transmission conditions are given by (2.3) below. This type of interface describes soft thin adhesive joints.
3. *Imperfect stiff interfaces* correspond to thin interphase layers of high rigidity. Here we distinguish between two situations. In the first case, the thin layer is 'replaced' by transmission conditions including a continuity condition for the displacement and a jump condition for the tractions; the corresponding transmission conditions are given by (2.11) and (2.15). In the second case, the highly rigid interphase layer also has a high mass density, the displacements $u^\pm$ are continuous across the interface $u^+(x, 0+, t) = u^-(x, 0-, t) = u(x, t)$ and the function $u(x, t)$ satisfies the wave equation (2.18).

2.2 *Weak interface*

Here we assume that the shear modulus of the material in Π_ε is small, so that $\mu = \varepsilon\mu_w$, where μ_w is of the same order of magnitude as $\mu_\pm$.

To leading order, the transmission conditions for the displacements $u^{\pm}$ can be written in the form (for $V < \min(v, v_+, v_-)$)

$$\mu_+ \frac{\partial u^+}{\partial y}\bigg|_{y=0+} = \mu_- \frac{\partial u^-}{\partial y}\bigg|_{y=0-}, \quad \mu_+ \frac{\partial u^+}{\partial y}\bigg|_{y=0+} = \tau_w (u^+|_{y=0+} - u^-|_{y=0-}), \tag{2.3}$$

where

$$\tau_w = \mu_w / h_0 = \mu / h. \tag{2.4}$$

Static problems with transmission conditions of this type were studied in (**1** to **5**).

In the following text, we assume that the crack moves with a constant speed $V < \min(v, v_+, v_-)$ which, in particular, implies that

$$V < v = \sqrt{\mu/\rho} = \sqrt{\varepsilon \mu_w / \rho}. \tag{2.5}$$

This suggests that the material of the interface has a small density, $\rho = \varepsilon \rho_w$, where $\rho_w = \mathcal{O}(\rho_\pm)$.

2.3 *Stiff interface*

Type I. For a stiff interface, it is assumed that

$$\mu = \mu_s / \varepsilon, \quad \text{and} \quad \rho = \rho_s / \varepsilon, \tag{2.6}$$

where μ_s has the same order of magnitude as $\mu_\pm$, and ρ_s is of the same order as $\rho_\pm$.

It will be shown that in this case the contact conditions for tractions are inhomogeneous. To see this, we need several terms of the asymptotic expansion of u and $u^{\pm}$. Let

$$u^{\pm}(x, y, t, \varepsilon) = u_0^{\pm}(x, y, t) + \varepsilon u_1^{\pm}(x, y, t) + \varepsilon^2 u_2^{\pm}(x, y, t) + \cdots, \tag{2.7}$$

$$u(x, \zeta, t, \varepsilon) = u_0(x, \zeta, t) + \varepsilon u_1(x, \zeta, t) + \varepsilon^2 u_2(x, \zeta, t) + \cdots, \tag{2.8}$$

where $\zeta = y/\varepsilon$ is the scaled variable of the cross-section of Π_ε.

It follows from the second condition of (2.2) that

$$\frac{\mu_s}{\varepsilon^2}\left(\frac{\partial u_0}{\partial \zeta} + \varepsilon \frac{\partial u_1}{\partial \zeta} + \varepsilon^2 \frac{\partial u_2}{\partial \zeta} + \cdots\right)\bigg|_{\zeta = \pm h_0/2} = \mu_\pm \frac{\partial u_0^{\pm}}{\partial y}\bigg|_{y=0\pm} + \cdots = \mathcal{O}(1), \tag{2.9}$$

which implies that

$$\frac{\partial u_0}{\partial \zeta}\bigg|_{\zeta = \pm h_0/2} = 0. \tag{2.10}$$

From the equation of motion it follows that the leading term $u_0(x, \zeta, t)$ is linear in ζ. Together with (2.10), this implies that u_0 is ζ-independent, and hence we have continuity at the interface for the displacements $u^{\pm}$, that is,

$$u_0(x, t) = u_0^+(x, 0+, t) = u_0^-(x, 0-, t). \tag{2.11}$$

Similarly to the leading term u_0, the function u_1 is also ζ-independent. The displacement transmission conditions yield

$$u_1^+(x, 0+, t) - u_1^-(x, 0-, t) = -\frac{h_0}{2}\left(\frac{\partial}{\partial y} u_0^+(x, 0+, t) + \frac{\partial}{\partial y} u_0^-(x, 0-, t)\right). \tag{2.12}$$

For the function u_2 inside the layer we derive the equation

$$\frac{\partial^2 u_2}{\partial \zeta^2} = -\frac{\partial^2 u_0}{\partial x^2} + \frac{1}{\upsilon^2}\frac{\partial^2 u_0}{\partial t^2}, \tag{2.13}$$

where $\upsilon = \sqrt{\mu_s/\rho_s}$. The right-hand side of (2.13) does not depend on ζ, and hence

$$\left.\frac{\partial u_2}{\partial \zeta}\right|_{\zeta=h_0/2} - \left.\frac{\partial u_2}{\partial \zeta}\right|_{\zeta=-h_0/2} = h_0\left(-\frac{\partial^2 u_0}{\partial x^2} + \frac{1}{\upsilon^2}\frac{\partial^2 u_0}{\partial t^2}\right). \tag{2.14}$$

Taking into account (2.9) we deduce the following transmission condition:

$$\left.\mu_+\frac{\partial u_0^+}{\partial y}\right|_{y=0+} - \left.\mu_-\frac{\partial u_0^-}{\partial y}\right|_{y=0-} = \left.\mu_s h_0\left(\frac{1}{\upsilon^2}\frac{\partial^2 u_0^+}{\partial t^2} - \frac{\partial^2 u_0^+}{\partial x^2}\right)\right|_{y=0+}. \tag{2.15}$$

Type II. It is also possible to increase the stiffness of the interface and address the issue of the corresponding transmission conditions and equations describing such a structure. The interface will be referred to as a 'stiff interface of type II', or rigid interface.

We assume that the thickness is the same as above, but the stiffness parameter is defined by $\mu = \varepsilon^{-2}\mu_s$, which is large compared to (2.6), and we also allow the interface to have high mass density $\rho = \varepsilon^{-2}\rho_s$.

We use the asymptotic approximations (2.7) and (2.8). The functions u_0 and u_1 are ζ-independent, and u_2 satisfies (2.13). The contact condition (2.9) is replaced by

$$\left.\frac{\mu_s}{\varepsilon^3}\left(\frac{\partial u_0}{\partial \zeta} + \varepsilon\frac{\partial u_1}{\partial \zeta} + \varepsilon^2\frac{\partial u_2}{\partial \zeta} + \cdots\right)\right|_{\zeta=\pm h_0/2} = \left.\mu_\pm\frac{\partial u_0^\pm}{\partial y}\right|_{y=0\pm} + \cdots = \mathcal{O}(1), \tag{2.16}$$

which implies (2.10) and

$$\left.\frac{\partial u_1}{\partial \zeta}\right|_{\zeta=\pm h_0/2} = 0, \quad \left.\frac{\partial u_2}{\partial \zeta}\right|_{\zeta=\pm h_0/2} = 0. \tag{2.17}$$

Hence, the functions u_0, u_1, u_2 are independent of ζ, and (2.13) is reduced to

$$\frac{\partial^2 u_0}{\partial x^2} - \frac{1}{\upsilon^2}\frac{\partial^2 u_0}{\partial t^2} = 0 \tag{2.18}$$

(compare with (2.14)). The jump in tractions for $u_0^\pm$ will be linked to the terms of higher order in the asymptotic approximation (2.7).

3. Formulation of model problems

We consider an infinite plane which consists of two half-planes $\Omega_\pm = \{(x, y): -\infty < x < \infty, \pm y > 0\}$, as shown in Fig. 2. The materials occupying the half-planes $\Omega_\pm$ are linearly elastic and isotropic, with shear moduli $\mu_\pm$ and densities $\rho_\pm$. We assume that a semi-infinite crack $M = \{(x, y): y = 0, x < Vt\}$ moves with a constant speed $V < \min\{\upsilon_+, \upsilon_-, \upsilon\}$ in the positive direction of the x-axis. The displacements $u^\pm$ satisfy the equations of motion in $\Omega_\pm$ (see (2.1)), the traction

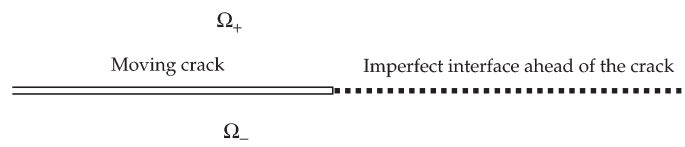

Fig. 2 Composite plane with a crack moving along an imperfect interface

conditions on the crack surfaces

$$\mu_\pm \frac{\partial u^\pm}{\partial y}\bigg|_{y=0\pm} = g_\pm(Vt - x), \quad x < Vt, \tag{3.1}$$

and one of the four types of transmission conditions (discussed in section 2.1) posed at the interface ahead of the moving crack $x > Vt$. The functions $g_\pm$ in (3.1) describe a self-balanced external load which is applied to the crack surfaces and moves with a constant speed V together with the crack tip; these functions are chosen in such a way that they decay sufficiently fast at infinity.

Assume that the displacement field has the form $u^\pm(x, y, t) = u^\pm(x - Vt, y)$ in $\Omega_\pm$, and at every fixed time t it possesses a finite energy:

$$\mathcal{E}(u) = \int_{\Omega_+} \left(v_+^2 |\nabla u^+|^2 + (\dot{u}^+)^2\right) dx\, dy + \int_{\Omega_-} \left(v_-^2 |\nabla u^-|^2 + (\dot{u}^-)^2\right) dx\, dy < \infty. \tag{3.2}$$

We shall use a new system of coordinates (X, y) moving with speed V together with the crack tip such that $(X, y) = (x - Vt, y)$. In the new coordinates, the equations of motion take the form

$$\frac{\partial^2 u^\pm}{\partial X^2} + a_\pm^2 \frac{\partial^2 u^\pm}{\partial y^2} = 0, \tag{3.3}$$

where

$$a_\pm = \sqrt{\frac{\mu_\pm}{\mu_\pm - V^2\rho_\pm}} = \frac{v_\pm}{\sqrt{v_\pm^2 - V^2}}. \tag{3.4}$$

Also, we shall use the notation

$$a = \sqrt{\frac{\mu}{\mu - V^2\rho}} = \frac{v}{\sqrt{v^2 - V^2}}. \tag{3.5}$$

The boundary conditions (3.1) are then written as

$$\mu_\pm \frac{\partial u^\pm}{\partial y}\bigg|_{y=0\pm} = g_\pm(-X), \quad X < 0. \tag{3.6}$$

The transmission conditions ahead of the moving crack are written as follows.

- For an ideal contact interface

$$u^+(X, 0+) = u^-(X, 0-), \quad \mu_+ \frac{\partial u^+}{\partial y}(X, 0+) = \mu_- \frac{\partial u^-}{\partial y}(X, 0-), \quad X > 0. \tag{3.7}$$

- For a weak interface

$$\mu_+\frac{\partial u^+}{\partial y}(X,0+)=\mu_-\frac{\partial u^-}{\partial y}(X,0-),$$
$$\mu_+\frac{\partial u^+}{\partial y}(X,0+)=\tau_w(u^+(X,0+)-u^-(X,0-)) \tag{3.8}$$

  for $X>0$, and τ_w given by (2.4).

- For a stiff interface of type I

$$u^+(X,0+)-u^-(X,0-)=0,$$
$$\mu_+\frac{\partial u^+}{\partial y}(X,0+)-\mu_-\frac{\partial u^-}{\partial y}(X,0-)+\frac{\tau_s}{a^2}\frac{\partial^2 u^+}{\partial X^2}(X,0+)=0 \tag{3.9}$$

  for $X>0$, and $\tau_s=\mu_s h_0=\mu h$.

- For a stiff interface of type II (rigid interface)

$$u^+(X,0+)-u^-(X,0-)=0,\quad \frac{\partial^2 u^+}{\partial X^2}(X,0+)=0,\quad X>0. \tag{3.10}$$

  This is consistent with the description of a rigid inclusion (see, for example, (**8**)).

In the moving frame, the energy functional (3.2) can be represented by the formula

$$\mathcal{E}(u)=\int_{\Omega_+}\left(v_+^2|\nabla u^+|^2+V^2(u_X^+)^2\right)dX\,dy+\int_{\Omega_-}\left(v_-^2|\nabla u^-|^2+V^2(u_X^-)^2\right)dX\,dy. \tag{3.11}$$

The energy functional (3.11) is finite if the functions $u^\pm$ are chosen in such a way that

$$\nabla u^\pm(X,y)=\mathcal{O}(r^{\gamma_0-1}(\ln r)^p),\quad r\to 0,\quad \nabla u^\pm(X,y)=\mathcal{O}(r^{-\gamma_\infty-1}(\ln r)^q),\quad r\to\infty, \tag{3.12}$$

where $r=\sqrt{X^2+y^2}$, $\mathrm{Re}(\gamma_0)>0$, $\mathrm{Re}(\gamma_\infty)>0$, and p, q are integers. In addition, we assume that

$$u^\pm(X,y)=U^\pm+\mathcal{O}(r^{\gamma_0}(\ln r)^p),\quad r\to 0,\quad u^\pm(X,y)=\mathcal{O}(r^{-\gamma_\infty}(\ln r)^q),\quad r\to\infty. \tag{3.13}$$

The second condition in (3.13) eliminates arbitrary additive constants in the representation of solutions to the model boundary-value problems described above.

4. Integral representations

First, we introduce the coordinate transformations, $X_\pm=a_\pm X$, above and below the interface, respectively. Equations (3.3) in the upper and lower half-planes then take the form

$$\frac{\partial^2 u^\pm}{\partial X_\pm^2}+\frac{\partial^2 u^\pm}{\partial y^2}=0,\quad (X_\pm,y)\in\Omega_\pm. \tag{4.1}$$

The boundary conditions (3.6) at the crack surfaces are

$$\mu_\pm\frac{\partial u^\pm}{\partial y}\bigg|_{y=0\pm,\ X<0}=-\mu_\pm\frac{1}{r_\pm}\frac{\partial u^\pm}{\partial\theta_\pm}\bigg|_{\theta_\pm=\pm\pi}=g_\pm(r_\pm/a_\pm), \tag{4.2}$$

where $(r_\pm,\theta_\pm)$ are polar coordinates defined in $\Omega_\pm$: $X_\pm=r_\pm\cos\theta_\pm$, $y=r_\pm\sin\theta_\pm$, $\pm\theta_\pm\in(0,\pi)$.

The applied loads $g_\pm$ are self-balanced, that is,

$$\int_0^\infty g_+(X)\,dX = \int_0^\infty g_-(X)\,dX. \tag{4.3}$$

This implies that

$$\mu_\pm \int_{-\infty}^{\infty} \frac{\partial u^\pm}{\partial y}\bigg|_{y=0\pm} dX_\pm = \mu_\pm \int_0^\infty \left[-\frac{1}{r_\pm}\frac{\partial u^\pm}{\partial \theta_\pm}\bigg|_{\theta_\pm=\pm\pi} + \frac{1}{r_\pm}\frac{\partial u^\pm}{\partial \theta_\pm}\bigg|_{\theta_\pm=0\pm} \right] dr_\pm = 0 \tag{4.4}$$

or, taking into account (4.2),

$$\int_0^\infty \left[\mu_\pm \frac{1}{r_\pm}\frac{\partial u^\pm}{\partial \theta_\pm}\bigg|_{\theta_\pm=0\pm} + g_\pm(r_\pm/a_\pm) \right] dr_\pm = 0. \tag{4.5}$$

The Mellin transforms $\tilde{u}^\pm$ of the solutions $u^\pm$ of (4.1) have the form

$$\tilde{u}^\pm(s,\theta_\pm) = A_\pm(s)\cos(\theta_\pm s) + B_\pm(s)\sin(\theta_\pm s), \tag{4.6}$$

where $\tilde{u}^\pm$ are defined as follows:

$$\tilde{u}^\pm(s,\theta_\pm) = \int_0^\infty u^\pm(r_\pm,\theta_\pm) r_\pm^{s-1} dr_\pm. \tag{4.7}$$

The boundary conditions (4.2) yield

$$-s\mu_\pm[\mp A_\pm(s)\sin(\pi s) + B_\pm(s)\cos(\pi s)] = a_\pm^{s+1}\tilde{g}_\pm(s+1), \tag{4.8}$$

and the balance condition (4.3) takes the form

$$\tilde{g}_+(1) = \tilde{g}_-(1). \tag{4.9}$$

The constraints (3.12) and (3.13) imply that the functions $\tilde{u}^\pm(s,\cdot)$ are analytic in a strip $0 < \mathrm{Re}(s) < \gamma_\infty$, whereas $s\tilde{u}^\pm(s,\cdot)$ and $\partial\tilde{u}^\pm(s,\theta_\pm)/\partial\theta_\pm$ are analytic in a wider strip $-\gamma_0 < \mathrm{Re}(s) < \gamma_\infty$. Also, the relation (4.5) implies

$$\lim_{s\to 0} \mu_\pm a_\pm^{-1} s B_\pm(s) = -\tilde{g}_\pm(1). \tag{4.10}$$

Finally, the integral representations for the functions $u^\pm$ have the form

$$u^\pm(r_\pm,\theta_\pm) = \frac{1}{2\pi i}\int_{-i\infty+\alpha}^{i\infty+\alpha} \{A_\pm(s)\cos(\theta_\pm s) + B_\pm(s)\sin(\theta_\pm s)\} r_\pm^{-s} ds, \tag{4.11}$$

where $0 < \alpha < \gamma_\infty$ is a real constant.

5. Asymptotics for cracks along imperfect interfaces

The problems are reformulated in terms of singular integral equations. We analyse solutions of these equations and derive new asymptotic representations for the displacement field near the tip of a steady-state crack moving along an imperfect interface.

5.1 *Imperfect weak interface*

We begin with the case of a weak interface and introduce the following notation:

$$D_1(s) = \mu_+ \frac{\partial}{\partial \theta_+} \tilde{u}^+(s, 0+) = \mu_+ s a_+^{-s-1} B_+(s). \tag{5.1}$$

LEMMA 5.1 *The function $D_1(s)$ is analytic in a strip $-1 < \mathrm{Re}(s) < \gamma_\infty$ and satisfies the functional equation*[†]

$$\tau_1 D_1(s-1) - \frac{1}{s}\cot(\pi s) D_1(s) = \frac{1}{s \sin(\pi s)} G_1(s), \quad 0 < \mathrm{Re}(s) < \gamma_\infty, \tag{5.2}$$

where γ_∞ is a non-negative constant, and $D_1(0) = -G_1(0) = -\tilde{g}_\pm(1)$. Here τ_1 is a non-dimensional constant,

$$\tau_1 = \frac{\tau_w^{-1}\mu_+\mu_-}{a_-\mu_+ + a_+\mu_-}, \tag{5.3}$$

and the function G_1 is analytic in a domain containing the strip $-1 < \mathrm{Re}(s) < \gamma_\infty$, and it is defined by the formula

$$G_1(s) = \frac{a_+\mu_-\tilde{g}_+(s+1) + a_-\mu_+\tilde{g}_-(s+1)}{a_-\mu_+ + a_+\mu_-}. \tag{5.4}$$

Proof. According to (3.8), the transmission conditions across the imperfect weak interface can be written in polar coordinates $(r_\pm, \theta_\pm)$ as follows:

$$\mu_+ \frac{1}{r_+} \frac{\partial u^+(r_+, \theta_+)}{\partial \theta_+}\bigg|_{\theta_+ = 0+} = \mu_- \frac{1}{r_-} \frac{\partial u^-(r_-, \theta_-)}{\partial \theta_-}\bigg|_{\theta_- = 0-}, \tag{5.5}$$

$$\tau_w \big(u^+(r_+, 0+) - u^-(r_-, 0-)\big) = \mu_+ \frac{1}{r_+} \frac{\partial u^+(r_+, \theta_+)}{\partial \theta_+}\bigg|_{\theta_+ = 0+}. \tag{5.6}$$

Using the identity $r_+/r_- = a_+/a_-$ and applying the Mellin transform to (5.5), we obtain

$$\mu_+ a_+^{-(s+1)} \frac{\partial \tilde{u}^+(s, \theta_+)}{\partial \theta_+}\bigg|_{\theta_+ = 0+} = \mu_- a_-^{-(s+1)} \frac{\partial \tilde{u}^-(s, \theta_-)}{\partial \theta_-}\bigg|_{\theta_- = 0-}. \tag{5.7}$$

The representation (4.6) yields

$$s\mu_+ a_+^{-(s+1)} B_+(s) = s\mu_- a_-^{-(s+1)} B_-(s), \tag{5.8}$$

where the functions $s B_\pm(s)$ are analytic in a strip $-\gamma_0 < \mathrm{Re}(s) < \gamma_\infty$.

Similarly, the second transmission condition (5.6) gives

$$\tilde{u}^+(s, 0+) - (a_+/a_-)^s \tilde{u}^-(s, 0-) = \tau_w^{-1}\mu_+ \frac{\partial \tilde{u}^+}{\partial \theta}(s-1, 0+). \tag{5.9}$$

[†] Matrix analogues of equations of this type were studied by a different method in (**16**).

The solutions $u^{\pm}$ are sought in the class of functions with the following asymptotics:

$$u^{\pm} = U_{\pm}^{(w)} + \Phi_{\pm}(\theta) r_{\pm}^{\gamma_0} \ln r_{\pm} + O(r_{\pm}), \quad r \to 0, \quad u^{\pm} = \mathcal{O}(r_{\pm}^{-\gamma_\infty}), \quad r_{\pm} \to \infty, \tag{5.10}$$

where $U_{\pm}^{(w)}$ are constants, and

$$\Phi'_{\pm}(0) = 0. \tag{5.11}$$

Thus, $p = 1, q = 0$ in (3.12), (3.13), and the functions $\tilde{u}^{\pm}(s, \theta_{\pm})$ and $(\partial\tilde{u}^{\pm}/\partial\theta_{\pm})(s, \theta_{\pm})$ are analytic in strips $0 < \mathrm{Re}(s) < \gamma_\infty$ and $-\gamma_0 < \mathrm{Re}(s) < \gamma_\infty$ respectively, whereas $(\partial\tilde{u}^{\pm}/\partial\theta_{\pm})(s, 0\pm)$ are analytic in a wider strip $-1 < \mathrm{Re}(s) < \gamma_\infty$. Equation (5.9) can be written as

$$a_+^{-s} A_+(s) - a_-^{-s} A_-(s) = \tau_w^{-1} \mu_+(s-1) a_+^{-s} B_+(s-1), \quad 0 < \mathrm{Re}(s) < \gamma_\infty. \tag{5.12}$$

Equations (4.8), (5.1), (5.8) and (5.12) lead to (5.2), with D_1 satisfying the constraint

$$-D_1(0) = G_1(0) = \tilde{g}_{\pm}(1), \tag{5.13}$$

the latter following from (4.9), (4.10), (5.1) and (5.4). The proof is complete.

Rearranging (5.2) gives

$$\tau_1 D_1(s-1) = \frac{D_1(s)\cos(s\pi) + G_1(s)}{s\sin(s\pi)}. \tag{5.14}$$

From (5.13) it then follows that the right-hand side of (5.14) has a simple pole at $s = 0$ and, therefore, $D_1(s)$ has a simple pole at $s = -1$. Rewriting (5.2) in the form

$$D_1(s) = [s\tau_1 D_1(s-1)\sin(s\pi) - G_1(s)]\sec(s\pi) \tag{5.15}$$

we deduce that the right-hand side of (5.15) has a simple pole at $s = \frac{1}{2}$. Consequently, for a solution of the functional equation (5.2) the constants γ_0 and γ_∞ can be chosen as follows:

$$\gamma_0 = 1, \quad \gamma_\infty = \tfrac{1}{2}. \tag{5.16}$$

5.1.1 *Reduction to a singular integral equation.* Let f_1 be a function whose Mellin transform satisfies the following equation:

$$D_1(s) = \Gamma(1+s)\left[\tilde{f}_1(s+1) - \frac{2}{\pi s}\, G_1(0)\right]\sin\frac{\pi s}{2}, \tag{5.17}$$

where $\Gamma(s)$ is the Euler gamma function. We note that $D_1(s)$ defined by (5.17) satisfies (5.13). Since $D_1(s)$ is analytic in the strip $-1 < \mathrm{Re}(s) < \frac{1}{2}$ and has simple poles at $s = -1$ and $s = \frac{1}{2}$, and $\Gamma(s+1)$ has a simple pole at $s = -1$, it follows that then $\tilde{f}_1(s+1)$ is analytic in a strip $-1-\delta < \mathrm{Re}(s) < \frac{1}{2}$ with $\delta > 0$.

LEMMA 5.2 *The function f_1 satisfies the singular integral equation*

$$f_1(\zeta) + \tau_1 k_1(\zeta) \int_0^{\infty} m_1(\zeta/\zeta')\, f_1(\zeta') d\zeta'/\zeta' = k_1(\zeta) n_1(\zeta), \quad 0 < \zeta < \infty, \tag{5.18}$$

where $n_1(\zeta)$ is the inverse Mellin transform of

$$\tilde{n}_1(s) = \frac{2}{\pi s} G_1(0) + \frac{2\tau_1 G_1(0)}{\pi(s-1)} \cot\frac{\pi s}{2} \tan(\pi s) - \frac{G_1(s)}{\Gamma(1+s)\cos(\pi s)\sin(\frac{1}{2}\pi s)}, \tag{5.19}$$

$$k_1(\zeta) = \frac{1}{\zeta + \tau_1} \quad \textit{and} \quad m_1(\zeta) = \frac{1}{2\pi i}\int_{-i\infty}^{i\infty} \frac{\zeta^s ds}{\cos(\pi s)} = \frac{\sqrt{\zeta}}{\pi(1+\zeta)}. \tag{5.20}$$

Proof. The function $\tilde{f}_1(s+1)$ solves the following functional equation:

$$\tilde{f}_1(s+1) + \tau_1 \tilde{f}_1(s)\left(\cot\frac{\pi s}{2}\tan(\pi s) - 1\right) + \tau_1 \tilde{f}_1(s) = \tilde{n}_1(s), \tag{5.21}$$

where $\tilde{n}_1(s)$ is the same as in (5.19). Applying the inverse Mellin transform gives (5.18).

From (5.21) it follows that the function $\tilde{f}_1(s)$ in (5.17) is analytic in the strip $-1 < \mathrm{Re}(s) < \frac{3}{2}$, and it decays as $\mathrm{Im}\,(s) \to \pm\infty$. The latter implies that

$$\int_0^\infty |f_1(\zeta)|\rho_{\alpha,\beta}(\zeta)\frac{d\zeta}{\zeta} < \infty, \quad \rho_{\alpha,\beta}(\zeta) = \begin{cases} \zeta^\alpha, & 0 < \zeta < 1, \\ \zeta^\beta, & 1 < \zeta < \infty, \end{cases} \tag{5.22}$$

with $\alpha > -1$ and $\beta < 1{\cdot}5$. Equation (5.18) is uniquely solvable in a class of functions specified by (5.22). Numerical methods and solvability results for equations of this class are discussed in (**17**).

For the purpose of illustration, in Fig. 3 we present the results of the numerical solution of (5.18). The diagram shows f_1 for different values of the crack tip velocity $V/\min\{v_-, v_+\} = 0,\ 0{\cdot}11, \ldots, 0{\cdot}99$. Since $\tilde{n}_1(s)$ decays as $\mathcal{O}(s^{-1})$ when $s \to \pm i\infty$ (see (5.19)), the solution f_1 of (5.18) is discontinuous at $\zeta = 1$. We note that the behaviour of f_1 shown in Fig. 3 is consistent with the asymptotic estimates of (**17**).

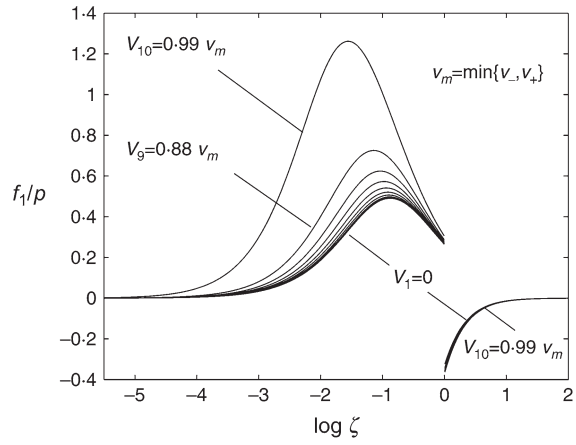

Fig. 3 Numerical solution of the integral equation (5.18) for different values of the crack tip velocity $V/\min\{v_-, v_+\} = 0, 0{\cdot}11, \ldots, 0{\cdot}99$, for a symmetric load $g_+(r) = g_-(r) = pe^{-r}$, with p constant

5.1.2 *Asymptotics near the crack tip and at infinity.* Here we use Lemmas 5.1 and 5.2 to obtain asymptotic approximations of the functions $u^{\pm}$ near the crack tip and at infinity.

THEOREM 5.1 (a) *In the vicinity of the crack tip, the asymptotic representation for* $u^{\pm}$ *is*

$$u^{\pm}(r_{\pm},\theta_{\pm}) = U_{\pm}^{(w)} \mp \frac{r_{\pm}}{\pi\,\mu_{\pm}}\Phi_1(\theta_{\pm},\ln r_{\pm}) + \mathcal{O}(r_{\pm}^2(\ln r_{\pm})^2), \quad r_{\pm}\to 0, \tag{5.23}$$

where

$$\begin{gathered} U_{\pm}^{(w)} = \frac{\pm a_{\pm}}{\pi\,\mu_{\pm}}\big[b_{00}+\tilde g'_{\pm}(1)\big], \\ \Phi_1 = \left\{ b_{10}\left[1-\ln\frac{r_{\pm}}{a_{\pm}}\right] + b_{11} - \tilde g_{\pm}(0)\right\}\cos\theta_{\pm} \mp\, b_{10}(\pi\mp\theta_{\pm})\sin\theta_{\pm}. \end{gathered} \tag{5.24}$$

(b) *Away from the crack tip, as* $r_{\pm}\to\infty$, *the displacement field has the approximation*

$$u^{\pm}(r_{\pm},\theta_{\pm}) = -\frac{2a_{\pm}^{3/2}}{\mu_{\pm}}b_{1\infty}r_{\pm}^{-1/2}\sin\frac{\theta_{\pm}}{2} + \mathcal{O}(r_{\pm}^{-1}), \quad r_{\pm}\to\infty. \tag{5.25}$$

In the formulae (5.24) *and* (5.25), $b_{00}, b_{10}, b_{1\infty}$ *and* b_{11} *are constant coefficients.*

Proof. Using formula (5.1), we can write the representation (4.11) in the form

$$u^{\pm}(r_{\pm},\theta_{\pm}) = \frac{\pm 1}{2\pi i}\int_{-i\infty+\alpha}^{i\infty+\alpha}\{D_1(s)\cos[(\pi\mp\theta_{\pm})s] + \tilde g_{\pm}(s+1)\cos(\theta_{\pm}s)\}\frac{a_{\pm}^{s+1}r_{\pm}^{-s}ds}{s\mu_{\pm}\sin(\pi s)}, \tag{5.26}$$

where $0<\alpha<\frac12$ is a real parameter. Within the strip $-1\leqslant \mathrm{Re}(s)<\frac12$, the integrand in (5.26) has a simple pole at $s=0$ and a double pole at $s=-1$. We deduce that the exponents γ_0 and γ_∞ in (5.10) are $\gamma_0=1$, $\gamma_\infty=\frac12$, and $p=1$, $q=0$. The function $D_1(s)$ admits the following asymptotic representations:

$$D_1(s) = \frac{b_{10}}{s+1} + b_{11} + \mathcal{O}(s+1) \quad \text{as } s\to -1, \qquad D_1(s) = \frac{b_{1\infty}}{s-\frac12} + \mathcal{O}(1) \quad \text{as } s\to \tfrac12,$$
$$D_1(s) = -G_1(0) + sb_{00} + \mathcal{O}(s^2) \quad \text{as } s\to 0,$$

where the coefficients are written in terms of the solution of (5.18), that is,

$$b_{10} = -\frac{2}{\pi}G_1(0) - \tilde f_1(0), \quad b_{11} = -\Gamma'(1)\left[\frac{2}{\pi}G_1(0) + \tilde f_1(0)\right] - \frac{2}{\pi}G_1(0) - \tilde f_1'(0), \tag{5.27}$$

$$b_{1\infty} = \frac{1}{\pi}\left\{G_1\big(\tfrac12\big) + \frac{\tau_1}{2}\sqrt{\frac{\pi}{2}}\left[\tilde f_1\big(\tfrac12\big) + \frac{4}{\pi}G_1(0)\right]\right\}, \quad b_{00} = \frac{\pi}{2}\,\tilde f_1(1) - G_1(0)\Gamma'(1).$$

Using the residue theorem we derive the asymptotic representations (5.23) and (5.25).

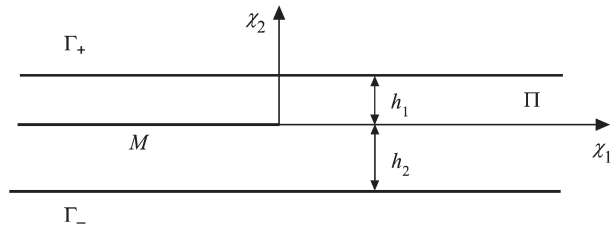

Fig. 4 Infinite layer with a crack

The direct computation of the gradient field shows that the components of the shear stress near the crack tip have a weak singularity of order $\mathcal{O}(\ln r_\pm)$. However, further observation shows that the traction is bounded at the interface $\theta_\pm = 0\pm$,

$$\mu_\pm \frac{1}{r_\pm}\frac{\partial u^\pm}{\partial \theta_\pm}\bigg|_{\theta_\pm=0\pm} = b_{10} + \mathcal{O}(r_\pm(\ln r_\pm)^2) \quad \text{as} \quad r_\pm \to 0. \tag{5.28}$$

From the asymptotic formula (5.23) we deduce that the displacement jump and the traction behave similarly as $r_\pm \to 0$, namely

$$u^+(r_+, 0+) - u^-(r_-, 0-) = \tau_1 b_{10} + \mathcal{O}(r_\pm(\ln r_\pm)^2) \quad \text{as} \quad r_\pm \to 0. \tag{5.29}$$

The latter is consistent with the transmission conditions (5.6).

We note that, on one hand, the asymptotic formula (5.23) does not involve the standard $\sqrt{r}$ asymptotic term typical for models of cracks in homogeneous elastic media. On the other hand, one can think of fracture of the weak interface as the formation of a crack within the thin layer, as illustrated in Fig. 4. In this case, the stress within the interphase layer will indeed be singular, and it is described by a model problem of the boundary-layer type for an infinite strip containing a crack. This problem is analysed in the following section, whose aim is to evaluate the coefficient near the singular term in the asymptotic approximation rather than to construct a uniform asymptotic expansion of the solution.

5.1.3 *Boundary layer analysis for a soft interface.* Assuming that we have solved the problem with the transmission conditions (2.3) and we know the limit values $u^\pm|_{y=0\pm} = U_\pm^{(w)}$ of the displacement at the crack tip, we then formulate a model problem in the scaled domain shown in Fig. 4.

Namely, we consider an auxiliary boundary-value problem for a Mode-III crack in a strip $\Pi = \{(\chi_1, \chi_2)\colon -\infty < \chi_1 < \infty, -h_2 < \chi_2 < h_1\}$. The crack propagates with a constant speed V along the χ_1-axis in such a way that at every finite time t it occupies the region $M = \{(\chi_1, \chi_2)\colon -\infty < \chi_1 < 0, \chi_2 = 0\}$; here we use a moving frame of reference with the origin at the crack tip. The displacement w then satisfies

$$\left(1 - \frac{V^2}{v^2}\right)\frac{\partial^2 w}{\partial \chi_1^2} + \frac{\partial^2 w}{\partial \chi_2^2} = 0 \quad \text{in } \Pi\backslash M, \tag{5.30}$$

the Dirichlet boundary conditions at the upper and lower surfaces $\Gamma_\pm$ of the strip Π

$$w(\chi_1, h_1) = U_+^{(w)}, \quad w(\chi_1, -h_2) = U_-^{(w)}, \quad -\infty < \chi_1 < \infty, \tag{5.31}$$

and the traction-free condition on the crack surfaces

$$\frac{\partial w}{\partial \chi_2}(\chi_1, 0_\pm) = 0, \quad \chi_1 < 0. \tag{5.32}$$

LEMMA 5.3 *The solution of the problem* (5.30) *to* (5.32) *has the asymptotic representation*

$$w(\chi_1, 0) = \frac{2}{\mu} K^{(w)} \sqrt{\chi_1} + \mathcal{O}(\chi_1) \quad \textit{as } \chi_1 \to 0+. \tag{5.33}$$

(a) *The coefficient* $K^{(w)}$ (*the Mode-*III *stress intensity factor*[‡]) *is given by*

$$K^{(w)} = \mu_w \frac{U_+^{(w)} - U_-^{(w)}}{\sqrt{a(h_1 + h_2)}}. \tag{5.34}$$

(b) *Comparing this result with the outer solution for a soft interface* (*see section* 5.1.2) *gives the following value for* b_{10}*:*

$$b_{10} = \sigma_0^* \equiv \mu_w [U_+^{(w)} - U_-^{(w)}]/(h_1 + h_2). \tag{5.35}$$

Proof. To find the solution of the above problem, we use the superposition principle, that is, we take $w = w^* + w^{(1)}$, where

$$w^* = \frac{U_+^{(w)} - U_-^{(w)}}{h_1 + h_2} \chi_2 + \frac{U_+^{(w)} h_2 + U_-^{(w)} h_1}{h_1 + h_2},$$

and $w^{(1)}$ solves the problem

$$\left(1 - \frac{V^2}{v^2}\right) \frac{\partial^2 w^{(1)}}{\partial \chi_1^2} + \frac{\partial^2 w^{(1)}}{\partial \chi_2^2} = 0 \quad \text{in } \Pi \setminus M, \tag{5.36}$$

$$w^{(1)}(\chi_1, h_1) = 0, \quad w^{(1)}(\chi_1, -h_2) = 0, \quad -\infty < \chi_1 < \infty, \tag{5.37}$$

$$\mu_w \frac{\partial w^{(1)}}{\partial \chi_2}(\chi_1, 0\pm) = -\sigma_0^*, \quad \chi_1 < 0. \tag{5.38}$$

To solve this problem, we apply the Fourier transform with respect to χ_1, $\mathcal{F}$. Using the boundary conditions (5.38) we derive the following functional equation for the Fourier transform W of the function $w^{(1)}$:

$$[W]_-(\xi_1) = \left(-\frac{i\sigma_0^*}{\xi_1 - i0} - F_+(\xi_1)\right) \hat{G}(\xi_1), \tag{5.39}$$

[‡] The Mode-III stress intensity factor is defined here by the relation $K_{\text{III}} = \mu \lim_{\chi_1 \to 0+} \partial w(\chi_1, 0)/\partial \chi_2$.

where

$$\hat{G}(\xi_1) = a(\tanh(\xi_1 h_1/a) + \tanh(\xi_1 h_2/a))/\xi_1,$$

$$[W]_-(\xi_1) = W(\xi_1, 0+) - W(\xi_1, 0-), \quad F_+(\xi_1) = \mu_w \frac{\partial W}{\partial \chi_2}(\xi_1, 0+) - \mathcal{F}\{-\sigma_0^* H(-\chi_1)\}.$$

The functions $[W]_-$ and F_+ are analytic in the upper half-plane $\mathrm{Im}\,(\xi_1) > -\eta$ and the lower half-plane $\mathrm{Im}\,(\xi_1) < \eta$ respectively, with η being a sufficiently small positive quantity.

The function $\hat{G}$ can be represented as follows:

$$\hat{G}(\xi_1) = \hat{G}_+(\xi_1)\hat{G}_-(\xi_1) = \frac{2a\psi_+^b(\xi_1)\psi_-^b(\xi_1)}{(\xi_1 - ib)_-^{1/2}(\xi_1 + ib)_+^{1/2}}, \quad \hat{G}_\pm(\xi_1) = \frac{\psi_\pm^b(\xi_1)\sqrt{2a}}{(\xi_1 \pm ib)_\pm^{1/2}}, \tag{5.40}$$

where for any $0 < \delta < b < [2\pi a/(h_1 h_2)]\max\{h_1, h_2\}$ we define

$$\psi_\pm^b(\xi_1) = \exp\left\{\frac{\pm 1}{2\pi i}\int_{-\infty\mp i\delta}^{\infty\mp i\delta} \frac{d\xi_1'}{\xi_1' - \xi_1} \ln\left[(2a)^{-1}(\xi_1' - ib)_-^{1/2}(\xi_1' + ib)_+^{1/2}\hat{G}(\xi_1')\right]\right\}.$$

Factorizing (5.39) (and taking into account (5.40)) we obtain

$$[W]_-(\xi_1) = -\frac{i\sigma_0^*}{\xi_1 - i0}\hat{G}_+(0)\hat{G}_-(\xi_1), \quad F_+(\xi_1) = -\frac{i\sigma_0^*}{\xi_1 - i0}\left(1 - \frac{\hat{G}_+(0)}{\hat{G}_+(\xi_1)}\right). \tag{5.41}$$

The function $F_+(\xi_1)$ admits the following asymptotic representation as $\xi_1 \to \infty$:

$$F_+(\xi_1) \sim \sqrt{\frac{i(h_1 + h_2)}{2a}}\frac{\sigma_0^*}{(\xi_1 + i0)_+^{1/2}}, \quad \xi_1 \to \infty,$$

from which it follows that the stress intensity factor $K^{(\omega)}$ at the crack tip has the form (5.34). Taking the limit as $\xi_1 \to 0$ in $(5.41)_1$ yields (5.35).

5.2 *Stiff imperfect interface*

Here we consider the transmission conditions (3.9), corresponding to the stiff interface of type I. In this case, the displacement is continuous across the interface, whereas the traction has a jump,

$$u^+(r_+, 0+) = u^-(r_-, 0-), \tag{5.42}$$

$$\mu_+\frac{1}{r_+}\frac{\partial u^+}{\partial \theta_+}(r_+, 0+) - \mu_-\frac{1}{r_-}\frac{\partial u^-}{\partial \theta_-}(r_-, 0-) = -\frac{a_+^2\tau_s}{a^2}\frac{\partial^2 u^+}{\partial r_+^2}(r_+, 0+). \tag{5.43}$$

The description of asymptotics for a stiff interface of type II will be given later as a particular case of the results formulated in this section. Applying the Mellin transform to (5.42) we obtain

$$a_+^{-s}A_+(s) = a_-^{-s}A_-(s), \quad 0 < \mathrm{Re}(s) < \gamma_\infty'. \tag{5.44}$$

Both functions $A_\pm(s)$ have simple poles at $s = 0$, that is,

$$A_+(s) = A_-(s) = s^{-1}\, U^{(s)} + \mathcal{O}(1), \quad s \to 0, \tag{5.45}$$

and therefore $sA_\pm(s)$ are analytic in a wider strip $-\gamma_0' < \mathrm{Re}(s) < \gamma_\infty'$. Define $D_2(s)$ by

$$D_2(s) = sa_\pm^{-s}\tilde{u}^\pm(s, 0\pm) = sa_\pm^{-s}A_\pm(s). \tag{5.46}$$

LEMMA 5.4 *The function $D_2(s)$ is analytic in the strip $-\frac{3}{2} < \mathrm{Re}(s) < 1$ and it satisfies the functional equation*[§]

$$\tau_2 D_2(s-1) + s^{-1}\tan(\pi s)D_2(s) = G_2(s)\sec(\pi s), \tag{5.47}$$

where

$$\tau_2 = \frac{\tau_s a_+ a_-}{a^2(\mu_+ a_- + \mu_- a_+)}, \quad G_2(s) = -\frac{a_+ a_-[\tilde{g}_-(s+1) - \tilde{g}_+(s+1)]}{s(\mu_+ a_- + \mu_- a_+)}, \tag{5.48}$$

and G_2 is a function analytic in a strip wider than that for D_2.

Proof. We show that $u^\pm$ admit asymptotic representations similar to (3.13), that is,

$$\begin{gathered} u^\pm = U^{(s)} + \Psi_\pm(\theta_\pm) r_\pm^{\gamma_0'} + \mathcal{O}(r_\pm^{\gamma_0'+1}\ln r_\pm) \quad \text{as } r_\pm \to 0, \\ u^\pm = \mathcal{O}(r_\pm^{-\gamma_\infty'}) \quad \text{as } r_\pm \to \infty, \end{gathered} \tag{5.49}$$

where $\Psi_\pm(0\pm) = 0$, and the exponents $\gamma_0', \gamma_\infty' > 0$ will be specified later. For a stiff interface, both p and q in (3.13) are equal to zero, and the functions $s\tilde{u}^\pm(s, 0\pm)$ are analytic in the strip $-1 - \gamma_0' < \mathrm{Re}(s) < \gamma_\infty'$.

In terms of the Mellin transforms, the transmission condition (5.43) is reduced to

$$\mu_+ sB_+(s) - \mu_- s(a_+/a_-)^{s+1}B_-(s) + s(s-1)(a_+/a)^2\tau_s A_+(s-1) = 0. \tag{5.50}$$

This equation is valid within the strip $-\gamma_0' < \mathrm{Re}(s) < \gamma_\infty' + 1$; here we have used the fact that $(s-1)A_+(s-1)$ does not have a pole at $s = 1$. Using (4.8) and (5.46), (5.50) can be written in the form (5.47). From (5.47) it follows that $D_2(s)$ is analytic in the strip $-\frac{3}{2} < \mathrm{Re}(s) < 1$.

The solution of (5.47) is taken in the form

$$D_2(s) = \Gamma(1+s)\cos(\pi s/2)\,\tilde{f}_2(s+1), \tag{5.51}$$

where $\tilde{f}_2(s+1)$ is analytic in the same strip as $D_2(s)$ and solves the functional equation

$$\tilde{f}_2(s+1) + \tau_2\,\tilde{f}_2(s) - \frac{\tau_2}{1+\cos(\pi s)}\,\tilde{f}_2(s) = \frac{G_2(s)}{\Gamma(s)\sin(\pi s)\cos(\pi s/2)}. \tag{5.52}$$

Thus, we arrive at the following conclusion.

[§] Equations of this type were also studied by a different method in (**10**, **18**).

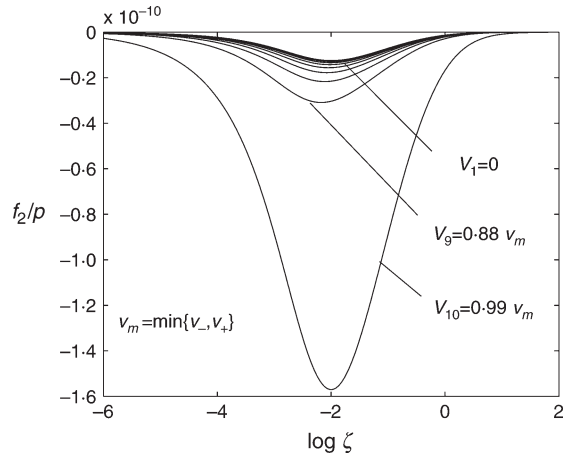

Fig. 5 Numerical solution of (5.53) for different values of the crack tip velocity $V/\min\{v_-, v_+\} = 0, 0{\cdot}11, \ldots, 0{\cdot}99$, for a non-symmetric load $g_+(r) = pe^{-r}$, $g_-(r) = pre^{-r}$, with p constant

LEMMA 5.5 *The inverse Mellin transform f_2 of $\tilde{f}_2$ satisfies the integral equation*

$$f_2(\zeta) + \tau_2 k_2(\zeta) \int_0^\infty m_2(\zeta/\zeta') f_2(\zeta') d\zeta'/\zeta' = k_2(\zeta) n_2(\zeta), \quad 0 < \zeta < \infty, \tag{5.53}$$

where $k_2(\zeta) = (\zeta + \tau_2)^{-1}$,

$$m_2(\zeta) = -\frac{1}{2\pi i} \int_{-i\infty}^{i\infty} \frac{\zeta^{-s} ds}{1 + \cos(\pi s)} = \frac{2}{\pi^2} \frac{\zeta \ln \zeta}{1 - \zeta^2}$$

and

$$n_2(\zeta) = \frac{1}{2\pi i} \int_{-i\infty}^{i\infty} \frac{G_2(s) \zeta^{-s} ds}{\Gamma(s) \sin(\pi s) \cos(\pi s/2)}.$$

Equation (5.53) is uniquely solvable in the class of functions specified by (5.22), with f_1 replaced by f_2, and $\alpha > -\frac{1}{2}$, $\beta < 2$ (**17**). The numerical solution of (5.53) is shown in Fig. 5. We note that, since the right-hand side of (5.53) is continuous, the solution f_2 is also continuous.

5.2.1 *Theorem on asymptotics*

THEOREM 5.2 (a) *As $r_\pm \to 0$, the asymptotic representation for $u^\pm$ takes the form*

$$u^\pm(r_\pm, \theta_\pm) = U^{(s)} + \frac{2}{\mu_\pm} K_\pm^{(s)} \sqrt{a_\pm r_\pm} \sin \frac{\theta_\pm}{2} + \mathcal{O}(r_\pm^{3/2} \ln r_\pm). \tag{5.54}$$

(b) *Away from the crack tip, as $r_\pm \to \infty$, the solution $u^\pm$ has the approximation*

$$u^\pm(r_\pm, \theta_\pm) = \frac{2a_\pm^{3/2}}{\pi \mu_\pm} b_\infty^{(s)\pm} r_\pm^{-1/2} \sin \frac{\theta_\pm}{2} + \mathcal{O}(r_\pm^{-1}). \tag{5.55}$$

In the formulae (5.54) *and* (5.55), $K_{\pm}^{(s)}$, $b_{\infty}^{(s)\pm}$ *and* $U^{(s)}$ *are given by*

$$U^{(s)} = D_2(0), \quad K_{\pm}^{(s)} = -\frac{1}{\pi}\left[\tilde{g}_{\pm}\left(\tfrac{1}{2}\right) \pm \frac{\mu_{\pm}}{a_{\pm}} D_2\left(-\tfrac{1}{2}\right)\right], \tag{5.56}$$

$$b_{\infty}^{(s)\pm} = -\tilde{g}_{\pm}\left(\tfrac{3}{2}\right) \pm \frac{\mu_{\pm}}{a_{\pm}} D_2\left(\tfrac{1}{2}\right),$$

$$D_2(0) = \tilde{f}_2(1), \quad D_2\left(-\tfrac{1}{2}\right) = \sqrt{\pi/2}\, \tilde{f}_2\left(\tfrac{1}{2}\right), \quad D_2\left(\tfrac{1}{2}\right) = \sqrt{\pi/8}\, \tilde{f}_2\left(\tfrac{3}{2}\right).$$

Proof. Using (5.46) the integral representation (4.11) can be written in the form

$$u^{\pm}(r_{\pm}, \theta_{\pm}) = \frac{1}{2\pi i} \int_{-i\infty+\alpha}^{i\infty+\alpha} \left\{ \frac{\mu_{\pm}}{a_{\pm}} D_2(s) \cos[(\pi \mp \theta_{\pm})s] - \tilde{g}_{\pm}(s+1) \sin(\theta_{\pm} s) \right\}$$

$$\times \frac{a_{\pm}^{s+1} r_{\pm}^{-s} ds}{s\mu_{\pm} \cos(\pi s)}, \tag{5.57}$$

where $0 < \alpha < \frac{1}{2}$ is a real parameter; this leads to (5.54) and (5.55). From (5.54) it follows that, for the transmission conditions of type I associated with an imperfect stiff interface, the leading-order asymptotic representations for stress do not include logarithmic terms (nevertheless, the logarithmic dependence may appear in higher-order approximations). The exponents in (5.49) are given by $\gamma_0' = \frac{1}{2}$ and $\gamma_{\infty}' = \frac{1}{2}$.

Let us note that the stress intensity factors $K_{\pm}^{(s)}$ are the same for a symmetric load, that is, when $g_+ = g_-$. In general, however, $K_+^{(s)} \neq K_-^{(s)}$, the traction is discontinuous across the interface ahead of the crack tip, and its jump admits the following asymptotic representation:

$$\sigma_{yz}^{+}(X, 0+) - \sigma_{yz}^{-}(X, 0-) = \frac{1}{\sqrt{X}}(K_+^{(s)} - K_-^{(s)}) + \mathcal{O}(\sqrt{X} \ln X) \quad \text{as } X \to 0+. \tag{5.58}$$

5.3 *Other interfaces*

Ideal interface. In this case the transmission conditions are given by (3.7). Let us note that these can be obtained from (3.8) or (3.9) by taking $\tau_w \to 0$ or $\tau_s \to 0$ respectively; the first problem is then singularly perturbed, whereas the second one is regularly perturbed. This allows us to use the results of section 4.2, with $\tau_2 = 0$. Thus, we derive the asymptotic representations

$$u^{\pm}(r_{\pm}, \theta_{\pm}) = U^{(i)} + \frac{2}{\mu_{\pm}} K^{(i)} \sqrt{a_{\pm} r_{\pm}} \sin\frac{\theta_{\pm}}{2} + \mathcal{O}(r_{\pm}) \quad \text{as } r_{\pm} \to 0, \tag{5.59}$$

$$u^{\pm}(r_{\pm}, \theta_{\pm}) = \frac{2a_{\pm}^{3/2}}{\pi\mu_{\pm}} b_{\infty}^{(i)} r_{\pm}^{-1/2} \sin\frac{\theta_{\pm}}{2} + \mathcal{O}(r_{\pm}^{-1}) \quad \text{as } r_{\pm} \to \infty, \tag{5.60}$$

where $U^{(i)}$, $K^{(i)}$ and $b_{\infty}^{(i)}$ are

$$U^{(i)} = \frac{a_+ a_-}{\pi(\mu_+ a_- + \mu_- a_+)}(\tilde{g}_+'(1) - \tilde{g}_-'(1)), \quad K^{(i)} = -\frac{1}{\pi} G_1\left(-\tfrac{1}{2}\right), \quad b_{\infty}^{(i)} = -G_1\left(\tfrac{1}{2}\right),$$

and G_1 is given by (5.4). We mention that $K^{(i)}$ depends on V for a non-symmetric load.

The above problem for a symmetric loading ($g_+ = g_- = g_{\rm sym}$) has been analysed by Freund (**14**) using the Wiener–Hopf method. In the symmetric case,

$$U^{(i)}_{\rm sym} = 0, \quad K^{(i)}_{\rm sym} = -\frac{1}{\pi}\,\tilde{g}_{\rm sym}\big(\tfrac{1}{2}\big), \quad b^{(i)}_{\infty} = -\tilde{g}_{\rm sym}\big(\tfrac{3}{2}\big), \tag{5.61}$$

and

$$u^{\pm}(r_{\pm}, 0\pm) = 0. \tag{5.62}$$

Stiff imperfect interface of type II (rigid interface). The transmission conditions (3.10), together with the assumption that the displacement field $u^{\pm}$ decays as $r_{\pm} \to \infty$, lead to the boundary conditions (5.62). The solution for a stiff interface of type II can be obtained either directly from the solution for an ideal interface or from the solution for a type I stiff interface by taking the limit as $\tau_2 \to \infty$. The asymptotic representations (5.59) and (5.60) hold in each half-plane $\mathbf{\Omega}_{\pm}$, with $U^{(i)}$, $K^{(i)}$ and $b^{(i)}_{\infty}$ replaced by $U^{(r)}$, $K^{(r)}_{\pm}$ and $b^{(r)\pm}_{\infty}$ respectively, where

$$U^{(r)} = 0, \quad K^{(r)}_{\pm} = -\pi^{-1}\,\tilde{g}_{\pm}\big(\tfrac{1}{2}\big), \quad b^{(r)\pm}_{\infty} = -\tilde{g}_{\pm}\big(\tfrac{3}{2}\big). \tag{5.63}$$

5.4 *Delamination on a stiff interface*

In this section we consider a problem of delamination on one side of the stiff interface. Instead of the semi-infinite crack, with Neumann boundary conditions on both faces (see Fig. 6(a)), we consider a region of delamination shown in Fig. 6(b). While ahead of the debonding region the transmission conditions are the same as in (5.42), (5.43), we have a new set of boundary conditions on the faces of the delamination region as described below.

Let us assume that the delamination process takes place only at one side of the stiff interface (see Fig. 6b). Then the corresponding boundary conditions take the form

$$-\mu_- \frac{1}{r_-}\frac{\partial u^-}{\partial \theta_-}\bigg|_{\theta_- = -\pi} = g_-(r_-/a_-), \tag{5.64}$$

$$-\mu_+ \frac{1}{r_+}\frac{\partial u^+}{\partial \theta_+}(r_+, \pi) - g_+(r_+/a_+) = -\frac{a_+^2 \tau_s}{a^2}\frac{\partial^2 u^+}{\partial r_+^2}(r_+, \pi). \tag{5.65}$$

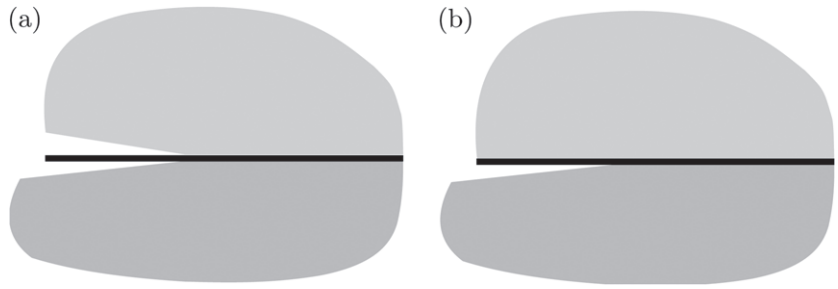

Fig. 6 Delamination of a stiff thin interface

Applying the Mellin transform to (5.42) we obtain (5.44); both functions $A_\pm(s)$ have simple poles at $s = 0$ (see (5.45)), and $sA_\pm(s)$ are analytic in a strip $-\gamma_0' < \mathrm{Re}(s) < \gamma_\infty'$, where $\gamma_0', \gamma_\infty'$ are positive constants.

The estimates (5.49) have to be satisfied with $\Psi_\pm(0\pm) = 0$, $\gamma_0', \gamma_\infty' > 0$. In addition, from (5.65) it follows that $\Psi_+(\pi) = 0$. The functions $s\tilde{u}^\pm(s, 0\pm)$ are analytic in a wider strip $-1 - \gamma_0' < \mathrm{Re}(s) < \gamma_\infty'$. The second transmission condition is reduced to (5.50).

The boundary condition (5.64) is the same as in (4.8), that is,

$$-s\mu_-[A_-(s)\sin(\pi s) + B_-(s)\cos(\pi s)] = a_-^{s+1}\tilde{g}_-(s+1), \tag{5.66}$$

while the second condition (5.65) can be written in the form

$$s\mu_+[A_+(s)\sin(\pi s) - B_+(s)\cos(\pi s)] - a_+^{s+1}\tilde{g}_+(s+1) = s(s-1)\frac{a_+^2}{a^2}\tau_s[A_+(s-1)\cos(\pi s) + B_+(s-1)\sin(\pi s)]. \tag{5.67}$$

Let us introduce the function $D_3(s)$ such that

$$D_3(s) = sa_+^{-s}\tilde{u}^+(s,\pi) = sa_+^{-s}[A_+(s)\cos(\pi s) + B_+(s)\sin(\pi s)]. \tag{5.68}$$

We shall also use $D_2(s)$ introduced earlier in (5.46). The functions $D_2(s)$, $D_3(s)$ have the common strip of analyticity $-1 - \gamma_0' < \mathrm{Re}(s) < \gamma_\infty'$. It is useful to note that $D_2(0) = D_3(0)$.

LEMMA 5.6 *The vector function* $\mathbf{D}(s) = [D_2(s), D_3(s)]^T$ *satisfies the functional equation*

$$\mathbf{D}(s) = \mathcal{A}(s)\Big\{\mathbf{G}(s) - s\frac{\tau_s}{a^2}\mathcal{B}(s)\mathbf{D}(s-1)\Big\}, \quad -\gamma_0' < \mathrm{Re}(s) < \gamma_\infty', \tag{5.69}$$

where

$$\mathcal{A}(s) = \beta\begin{bmatrix} -\dfrac{\mu_+}{a_+}\dfrac{1}{\sin(\pi s)} & \dfrac{\mu_+}{a_+}\dfrac{1}{\sin(\pi s)} \\ -\dfrac{\mu_+}{a_+}\dfrac{2}{\sin(2\pi s)} & \left(\dfrac{\mu_+}{a_+} + \dfrac{\mu_-}{a_-}\right)\dfrac{\kappa + \cos(2\pi s)}{\sin(2\pi s)} \end{bmatrix}, \quad \mathbf{G}(s) = \begin{bmatrix} \tilde{g}_-(s+1) \\ \tilde{g}_+(s+1) \end{bmatrix}, \tag{5.70}$$

$$\mathcal{B}(s) = \begin{bmatrix} -\cos(\pi s) & 0 \\ 0 & 1 \end{bmatrix}, \quad \kappa = \frac{\mu_+a_- - \mu_-a_+}{\mu_+a_- + \mu_-a_+}, \quad \beta = \left(\frac{\mu_+}{a_+}\left(\frac{\mu_+}{a_+} + \frac{\mu_-}{a_-}\right)\right)^{-1}. \tag{5.71}$$

Note that, due to the balance condition (4.9), the functions $\mathcal{A}(s)\mathbf{G}(s)$ and $s\mathcal{A}(s)$ are analytic at $s = 0$. By investigating a priori properties of a solution of (5.69) one can find that $D_2(s)$ does not have a pole at $s = \frac{1}{2}$, while $D_3(s)$ has a simple pole at $s = \frac{1}{2}$, that is,

$$D_3(s) = d_3/\big(s - \tfrac{1}{2}\big) + \mathcal{O}(1) \quad \text{as} \quad s \to \tfrac{1}{2}, \tag{5.72}$$

where

$$d_3 = \frac{a_+}{\pi\mu_+}G_1\big(\tfrac{1}{2}\big) - \frac{1}{2\pi}\frac{\mu_-}{a_-}\frac{\beta\tau_s}{a^2}D_3\big(-\tfrac{1}{2}\big). \tag{5.73}$$

Also, from (5.69) it follows that the functions $D_2(s)$ and $D_3(s)$ have a simple pole at $s = 1$.

The direct analysis of the solution gives

$$D_2(s-1) = d_2/\left(s+\tfrac{1}{2}\right) + \mathcal{O}(1) \quad \text{as} \quad s \to -\tfrac{1}{2}, \tag{5.74}$$

$$d_2 = \frac{2a^2}{\pi\,\tau_s}\left(\tilde{g}_-\left(\tfrac{1}{2}\right) - \frac{\mu_-}{a_-}\,D_2\left(-\tfrac{1}{2}\right)\right), \tag{5.75}$$

while $D_3(s-1)$ is analytic at $s=-\frac{1}{2}$. Also, $D_2(s-1)$ and $D_3(s-1)$ may have simple poles at $s=-1$:

$$D_2(s-1) = D_3(s-1) + \mathcal{O}(1) = \frac{a^2\mu_+}{\tau_s}\frac{d_1}{s+1} + \mathcal{O}(1), \quad s \to -1, \tag{5.76}$$

$$d_1 = -\frac{1}{\pi\,a_+}(D_2(-1) + D_3(-1)). \tag{5.77}$$

Thus, $D_2(s)$ and $D_3(s)$ are analytic for $-\frac{3}{2} < \mathrm{Re}(s) < 1$ and $-2 < \mathrm{Re}(s) < \frac{1}{2}$, respectively.

The solution of (5.69) is taken in the form

$$\mathbf{D}(s) = \Gamma(1+s)\cos\frac{\pi s}{2}\begin{bmatrix}1 & 0\\ 1 & \tan(\pi s)\tan(\frac{1}{2}\pi s)\end{bmatrix}\tilde{\mathbf{F}}(s+1) - \frac{a_+}{\mu_+}\begin{bmatrix}0 & 0\\ 0 & \tan(\pi s)\end{bmatrix}\mathbf{G}(s), \tag{5.78}$$

where $\tilde{\mathbf{F}}(s+1)$ is analytic in the same strip as $\mathbf{D}(s)$. It can be verified directly that in new notation (5.69) is equivalent to

$$\tilde{\mathbf{F}}(s+1) + \frac{\tau_d}{2}\begin{bmatrix}(\kappa+1) & 0\\ (\kappa-1) & 2\end{bmatrix}\tilde{\mathbf{F}}(s) - \frac{\tau_d}{2\cos(\pi s)}\begin{bmatrix}0 & (\kappa+1)\\ 0 & (\kappa-1)\end{bmatrix}\tilde{\mathbf{F}}(s) = \tilde{\mathbf{N}}(s), \tag{5.79}$$

where $\tau_d = \tau_s a_+(a^2\mu_+)^{-1}$ and

$$\tilde{\mathbf{N}}(s) = \frac{a_+(1+\kappa)}{2\mu_+\Gamma(s+1)\sin(\pi s)\cos(\frac{1}{2}\pi s)}\begin{bmatrix}-1 & 1\\ -1 & 1-\dfrac{2(1+\cos(\pi s))}{1+\kappa}\end{bmatrix}\begin{bmatrix}\tilde{g}_-(s+1)-\tilde{g}_+(s+1)\\ s\tau_d\tan(\pi s)\tilde{g}_+(s)\end{bmatrix}. \tag{5.80}$$

Finally, applying the inverse Mellin transform directly to (5.79), we obtain the following lemma.

LEMMA 5.7 *The vector function* $\mathbf{F} = [F_1, F_2]^T$ *solves the integral equation*

$$\mathbf{F}(\zeta) - \frac{\tau_d}{2}\mathbf{K}(\zeta)\begin{bmatrix}\kappa+1\\ \kappa-1\end{bmatrix}\int_0^\infty m_1(\zeta/\zeta')F_2(\zeta')\frac{d\zeta'}{\zeta'} = \mathbf{K}(\zeta)\mathbf{N}(\zeta),\ 0<\zeta<\infty, \tag{5.81}$$

where $\mathbf{N}(\zeta)$ *is the inverse Mellin transform of the vector function* $\tilde{\mathbf{N}}(\zeta)$ *and*

$$\mathbf{K}(\zeta) \equiv (\zeta\mathbf{I} + \mathcal{A}_0)^{-1} = \begin{bmatrix}\dfrac{2}{2\zeta+\tau_d(1+\kappa)} & 0\\ \dfrac{\tau_d(1-\kappa)}{(\zeta+\tau_d)(2\zeta+\tau_d(1+\kappa))} & \dfrac{1}{\zeta+\tau_d}\end{bmatrix}. \tag{5.82}$$

We note that the matrix of the system (5.81) is triangular. Thus, we first numerically solve the second integral equation for the function $F_2(\zeta)$ only,

$$F_2(\zeta) - \frac{\tau_d \zeta(\kappa-1)}{(\zeta+\tau_d)(2\zeta+\tau_d(1+\kappa))}\int_0^\infty m_1(\zeta/\zeta')F_2(\zeta')\frac{d\zeta'}{\zeta'} = \begin{bmatrix}0\\1\end{bmatrix}^T \mathbf{K}(\zeta)\mathbf{N}(\zeta),\ 0<\zeta<\infty. \quad (5.83)$$

This equation is uniquely solvable in a class of function with finite norm (5.22), with $\alpha > -\frac{1}{2}$, $\beta < 2$ (**17**). Then we find F_1 immediately:

$$F_1(\zeta) = \frac{\tau_d(\kappa+1)}{2\zeta+\tau_d(1+\kappa)}\int_0^\infty m_1(\zeta/\zeta')F_2(\zeta')\frac{d\zeta'}{\zeta'} + \begin{bmatrix}1\\0\end{bmatrix}^T \mathbf{K}(\zeta)\mathbf{N}(\zeta),\ 0<\zeta<\infty, \quad (5.84)$$

or, taking into account (5.83),

$$F_1(\zeta) = \frac{(\tau_d+\zeta)(\kappa+1)}{\zeta(\kappa-1)}\left\{F_2(\zeta) - \begin{bmatrix}0\\1\end{bmatrix}^T \mathbf{K}(\zeta)\mathbf{N}(\zeta)\right\} + \begin{bmatrix}1\\0\end{bmatrix}^T \mathbf{K}(\zeta)\mathbf{N}(\zeta). \quad (5.85)$$

Note that from (5.83) it follows that the term in braces in (5.85) decays as $\mathcal{O}(\zeta^2 \ln\zeta)$ when $\zeta \to 0$.

The results of numerical calculations are shown in Fig. 7. The functions F_1 (solid lines) and F_2 (dashed lines) are plotted for different values of $V/\min\{v_-, v_+\} = 0, 0{\cdot}11, \ldots, 0{\cdot}99$. Figure 7(a) corresponds to a symmetric load $g_+(r) = g_-(r) = pe^{-r}$, and Fig. 7(b) to a non-symmetric load $g_+(r) = pe^{-r}$, $g_-(r) = pre^{-r}$, with p constant.

We note that the integral equation (5.81) has non-trivial solutions for both symmetric and non-symmetric loads (compare with (5.53) which possesses a non-trivial solution for a non-symmetric load only).

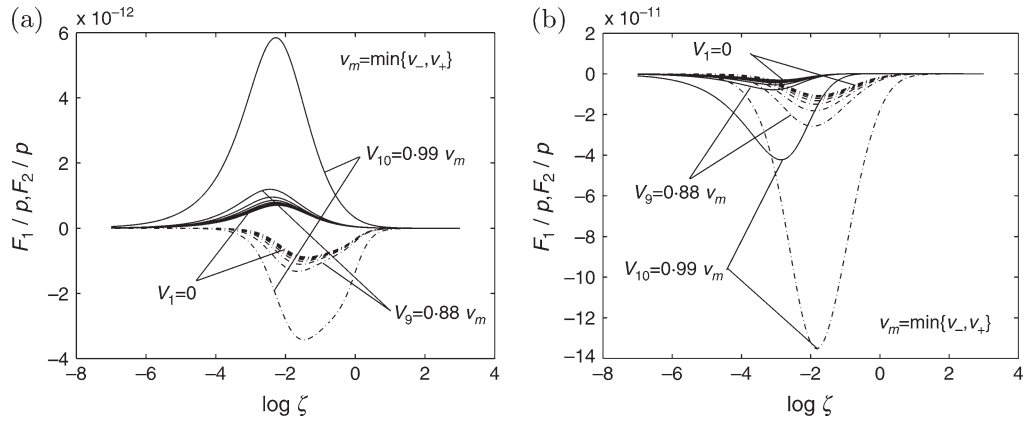

Fig. 7 The solutions F_1 (solid lines) and F_2 (dashed lines) of (5.83) and (5.84) for different values of the crack tip velocity $V/\min\{v_-, v_+\} = 0, 0{\cdot}11, \ldots, 0{\cdot}99$. (a) symmetric load; (b) non-symmetric load

5.4.1 *Theorem on asymptotics*

THEOREM 5.3 *The functions $u^{\pm}$ admit the following asymptotic representations:*

(a) *in the vicinity of the crack tip,*

$$u^+(r_+,\theta_+) = U^{(d)} + d_1 r_+ \sin\theta_+ + \frac{4}{3}\frac{a^2}{\tau_s}K_-^{(d)}\left(\frac{r_+}{a_+}\right)^{3/2}\cos\frac{3\theta_+}{2} + \mathcal{O}(r_+^2\ln r_+),\ r_+\to 0, \tag{5.86}$$

$$u^-(r_-,\theta_-) = U^{(d)} + \frac{2}{\mu_-}K_-^{(d)}\sqrt{a_-r_-}\sin\frac{\theta_-}{2} + \mathcal{O}(r_-^{3/2}\ln r_-),\ r_-\to 0, \tag{5.87}$$

where d_1 is given by (5.77)*, while the expressions for $U^{(d)}$, $K_-^{(d)}$ are similar to those for $U^{(s)}$, $K_-^{(s)}$ in* (5.56)*, with $D_2(s)$ being the first component of the solution* $\mathbf{D}(s)$ *of* (5.69)*;*

(b) *away from the crack tip,*

$$u^+(r_+,\theta_+) = -2\sqrt{\frac{a_+}{r_+}}d_3\sin\frac{\theta_+}{2} + \mathcal{O}(r_+^{-1}\ln r_+),\quad r_+\to\infty, \tag{5.88}$$

$$u^-(r_-,\theta_-) = -2\frac{a_-\mu_+}{a_+\mu_-}\sqrt{\frac{a_-}{r_-}}d_3\sin\frac{\theta_-}{2} + \mathcal{O}(r_-^{-1}\ln r_-),\quad r_-\to\infty, \tag{5.89}$$

with d_3 given by (5.73)*.*

Proof. The integral representation (4.11) in the domain Ω_+ can be written in the form

$$u^+(r_+,\theta_+) = \frac{1}{2\pi i}\int_{-i\infty+\alpha}^{i\infty+\alpha}\{D_2(s)\sin[(\pi-\theta_+)s] + D_3(s)\sin(\theta_+ s)\}\frac{a_+^s r_+^{-s}ds}{s\sin(\pi s)}, \tag{5.90}$$

where $0<\alpha<\frac{1}{2}$ is a real parameter; this leads to the asymptotic representations (5.86), (5.88) for the displacements u^+. From (5.86) it follows that ∇u^+ has no singularity near the crack tip.

The asymptotic formulae (5.87), (5.89) for the function u^- in the domain Ω_- follow immediately from the representation (5.57). The proof is complete.

6. Numerical simulations and concluding remarks

6.1 *Soft interface*

The numerical calculations for the weak interface were done for a thin epoxy adhesive interphase layer ($h = 0{\cdot}003$) surrounded by either iron above and titanium below or iron both above and below. The material parameters used in the calculations are given in Table 1.

Figure 8 shows the normalized displacement jump $[U^{(\omega)}](\tau_1(V),V)/[U^{(\omega)}](\tau_1(0),0)$ at the tip of a crack propagating along a weak interface for a symmetric load $g_\pm(r) = pe^{-r}$, where p is constant and τ_1 is given by (5.3). We consider two different cases: (1) both domains Ω_+ and Ω_- are made of iron, and (2) the domain Ω_+ is made of iron whereas Ω_- is made of titanium. Figure 8(a) presents the displacement jump as a function of the crack tip velocity V. One can see that the displacement jump increases monotonically with V and becomes unbounded as $V\to v_m \equiv \min\{v_+, v_-\}$. We note that the static limit ($V=0$) is consistent with the earlier results (**11** to **13**).

Table 1 Material parameters used in computations for a crack propagating along a weak interface

Material	Shear modulus [N/m^2]	Mass density [kg/m^3]	wave speed [m/sec]
Iron	82×10^9	7860	3230
Titanium	44×10^9	4506	3124
Epoxy adhesive	77×10^7	1380	747

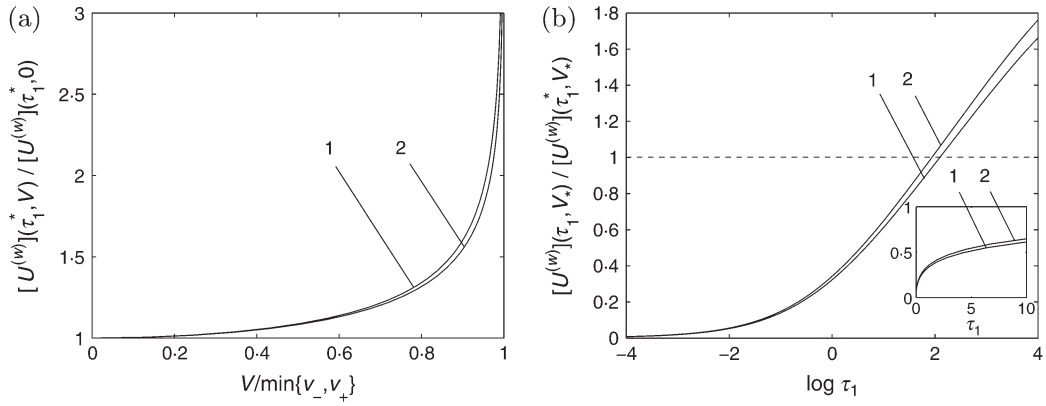

Fig. 8 The displacement jump at the tip of the crack propagating along a weak interface (curves 1 correspond to the case when both domains $\Omega_\pm$ are made of iron, curves 2 to the case when Ω_+ is made of iron and Ω_- of titanium). The diagram (a) shows the displacement jump as a function of the crack tip velocity V, whereas (b) corresponds to $V = v_m/2$. The insert on diagram (b) presents the displacement jump as a function of τ_1, whereas diagram (b) itself shows the displacement jump against $\log \tau_1$. Both diagrams were generated for a symmetric load $g_\pm = pe^{-r}$, with p constant

Figure 8(b) shows the dependence of the displacement jump on the elastic properties of the interphase layer. To generate the diagram we change the value of the parameter τ_w in the expression (5.3) for $\tau_1 = \tau_1(\tau_w, V)$ and take $V = V_* = \min\{v_-, v_+\}/2$, and $\tau_1^*(V) = \tau_1(\tau_w^*, V)$ for the epoxy adhesive from Table 1. As follows from Fig. 8(b) (see the insert) the displacement jump decays as $\mathcal{O}(\tau_1^{1/2})$ as $\tau_1 \to 0$, and thus $\sigma_{\theta z} = \mathcal{O}(\tau_1^{-1/2})$ as $\tau_1 \to 0$ (see (5.28) and (5.29)).

Figure 9 shows the stress intensity factor $K^{(w)}$ as a function of the normalized crack speed V for a crack propagating along a weak interface. Two cases are discussed: (a) the soft interface between similar materials (corresponding to the curves of group 1 in Fig. 8), and (b) the soft interface between dissimilar media (corresponding to the curves of group 2 in Fig. 8). First, we consider the epoxy adhesive interface as in Table 1. In this case $v = 0{\cdot}239 v_m$. Other weak interfaces of the same shear modulus but different material density (and therefore different wave speed v) are also analysed. In the case when $v < v_m = \min\{v_+, v_-\}$ the stress intensity factor is decreasing with the increase of the crack velocity V, and when $V \to v < v_m$ the stress intensity factor vanishes. Hence, in this case the crack has a tendency to slow down. When $v = v_m$, the change in the stress intensity

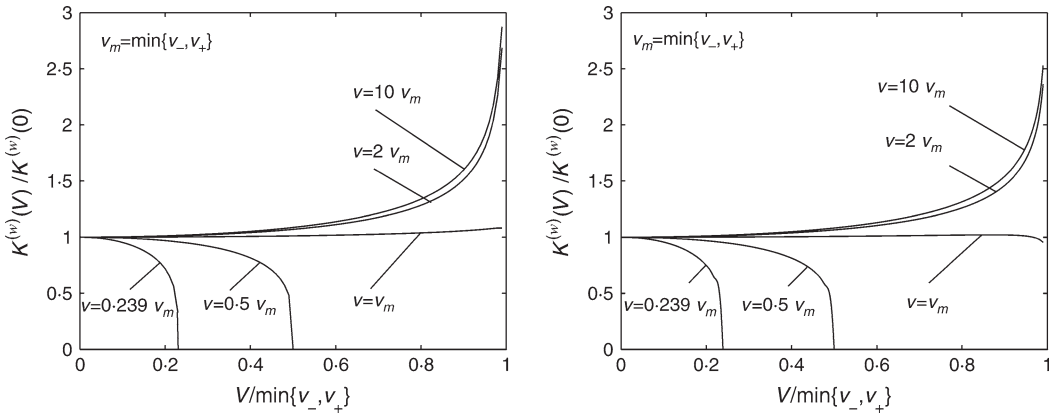

Fig. 9 Mode-III stress intensity factor $K^{(w)}$ for a crack propagating along a weak interface: the left diagram corresponds to the case when both domains $\Omega_\pm$ are made of iron, the right diagram is for when Ω_+ is made of iron and Ω_- of titanium. The applied load is the same as in Fig. 8

Table 2 Material parameters used in computations for a crack propagating along a stiff interface

Material	Shear modulus [N/m^2]	Mass density [kg/m^3]	wave speed [m/sec]
Iron (interface)	82×10^9	7860	3230
Magnesium	17×10^9	1738	3128
Aluminium	26×10^9	2700	3103

factor is negligibly small with the change of speed V, and it is similar to the stress intensity factor of the crack moving in a homogeneous material. When $v > v_m$ the stress intensity factor grows with speed, similarly to the growth of the displacement discontinuity $[U^{(w)}]$ (or the crack opening) depicted in Fig. 8. In the latter case, the crack opening $[U^{(w)}]$ can be used in the fracture criterion for a crack propagating along a weak interface. On the contrary, other cases of weak interfaces should use the stress intensity factors in the corresponding fracture criteria.

The presence of the boundary layer, where the stress field has a traditional square root singularity, resolves the issue of the energy transport for this problem. We remark that an alternative approach, implemented for the static case, was considered in (**19**).

6.2 *Stiff interface*

The computations for a stiff interphase are done for a thin iron layer surrounded by magnesium and aluminium. The material parameters are given in Table 2. In addition, we shall also investigate the case when the thin iron layer is situated between the aluminium half-planes.

In Fig. 10 we display the normalized stress intensity factors as functions of the crack speed; we note that the traction components are discontinuous across the interface; $K_\pm^{(s)}$ stand for the values

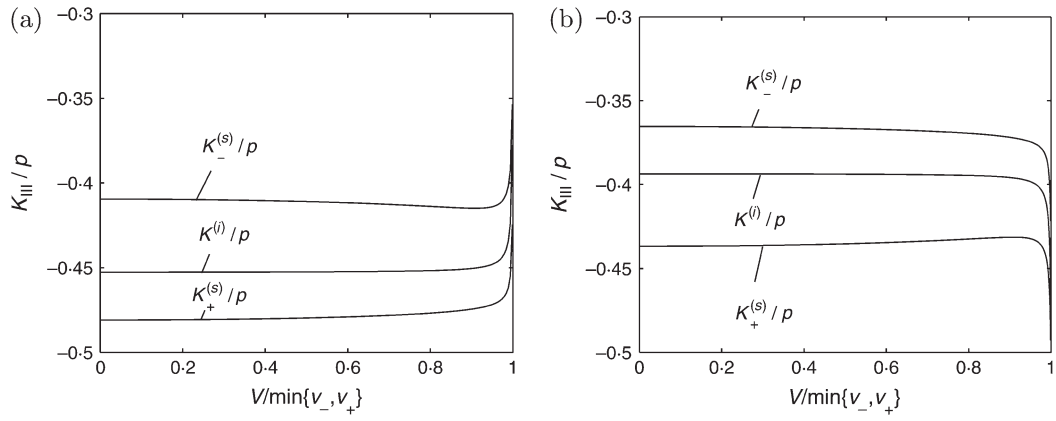

Fig. 10 Mode-III stress intensity factors $K_{\pm}^{(s)}$ (above and below the stiff interface) as functions of the crack tip speed V: the diagram (a) corresponds to the case when Ω_+ is made of magnesium and Ω_- of aluminium; the diagram (b) is for the case when we swap the two materials. The applied load is taken in the form $g_+ = pe^{-r}, g_- = pre^{-r}$, with p constant. The Mode-III stress intensity factor $K^{(i)}$ for an ideal interface is shown here for comparison

of the stress intensity factors above and below the stiff interface. For the sake of comparison, we also depict the stress intensity factor $K^{(i)}$ obtained for the case of an ideal contact (continuity of displacement components and tractions). The diagrams (a) and (b) contain different combinations of surrounding materials above and below the interface, for the case of a non-symmetric load defined as $g_+ = pe^{-r}, g_- = pre^{-r}$, with p constant. In both cases, the behaviour of the stress intensity factors is dominated by the load g_+. We note that for the case of a symmetric load, the values $K_{\pm}^{(s)}$ coincide with $K^{(i)}$.

In Fig. 11 we show the results of computations for the case of the symmetric distribution of materials around the interface: this diagram corresponds to the case of the iron interface surrounded by aluminium. The dashed lines in the diagram (b) represent the stress intensity factors $K_{\pm}^{(s)}$ for an additional special case of an interface that has the same shear modulus as iron but different density, so that the wave speed υ for the interphase layer is $\upsilon_m/2$.

Diagrams (a) and (b) in Fig. 12 correspond to the same load and distribution of the materials surrounding the interface as in Fig. 10. For the material of the interphase layer, we change the stiffness parameter τ_2 and depict the stress intensity factors $K_{\pm}^{(s)}$. It is shown that when τ_2 decreases the result, in the limit, corresponds to that for the ideal contact conditions, whereas the growth of τ_2 leads to the values $K_{\pm}^{(s)}$ for a perfectly rigid interface as defined by (5.63).

It is noted that the interchange of surrounding materials (with the same load in place) for the case of a stiff interface gives a finite change in the values of $K_{\pm}^{(s)}$, in contrast with the situation corresponding to the soft interface.

6.3 *Delamination crack on a stiff interface*

In this section we discuss the results of numerical computations for the case when the crack surface is loaded by the given traction on one side, and the other side of the crack surface is in contact with

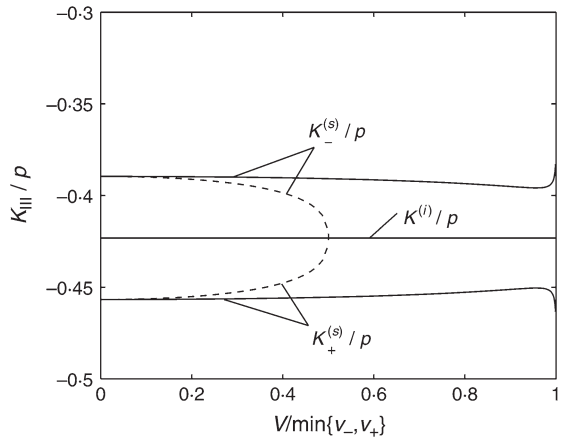

Fig. 11 Mode-III stress intensity factors $K_{\pm}^{(s)}$ (above and below the stiff interface) as functions of the crack tip speed V for the case when both Ω_+ and Ω_- are made of aluminium. The applied load is the same as in Fig. 10. The Mode-III stress intensity factor $K^{(i)}$ for an ideal interface is shown here for comparison

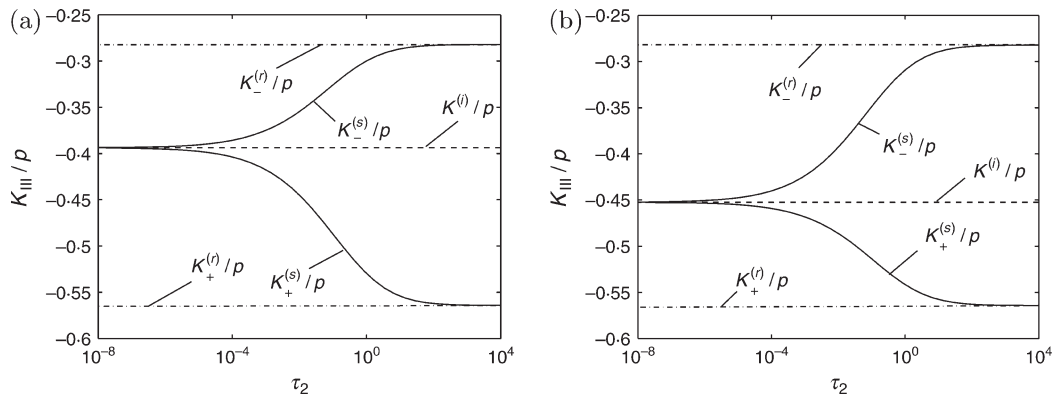

Fig. 12 Mode-III stress intensity factors $K_{\pm}^{(s)}$ (above and below the stiff interface) as functions of the parameter τ_2, for $V = \min\{v_-, v_+\}/2$: the diagram (a) corresponds to the case when Ω_+ is made of magnesium and Ω_- of aluminium, the diagram (b) is for the case when we swap the two materials. The applied load is the same as in Fig. 10. The Mode-III stress intensity factors $K^{(i)}$ (for an ideal interface) and $K_{\pm}^{(r)}$ (for a rigid interface) are shown here for comparison

the stiff interface and also subjected to the given load. The analytical study of this configuration is included in section 5.4. In this situation, the crack runs along the lower boundary of the interphase layer, and we classify this case as *delamination along a stiff interface* (see Fig. 6). For comparison, all graphs in Fig. 13 include the dashed lines (for $K_-^{(r)}/p$) corresponding to a perfectly rigid interface, so that the problem is equivalent to the one for a half-plane with the homogeneous Dirichlet

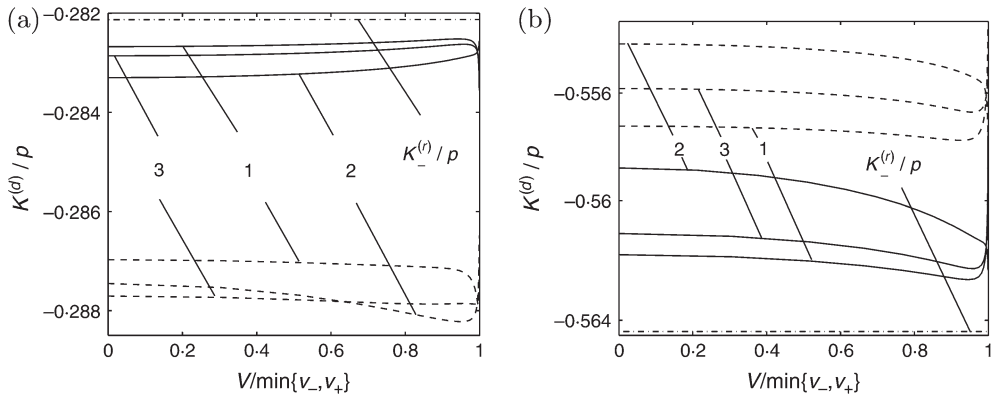

Fig. 13 Mode-III stress intensity factor $K^{(d)}$ for a delamination crack propagating below a stiff interface (curves 1: Ω_+ is made of aluminium, Ω_- of magnesium; curves 2: Ω_+ is made of magnesium, Ω_- of aluminium; curves 3: both $\Omega_\pm$ are made of aluminium). The diagram (a) corresponds to the symmetric load $g_\pm = pre^{-r}$, p is a constant (solid lines) and the non-symmetric load $g_+ = pe^{-r}, g_- = pre^{-r}$ (dashed lines). The diagram (b) corresponds to the other symmetric load: $g_\pm = pe^{-r}$ (solid lines) and the non-symmetric load: $g_+ = pre^{-r}, g_- = pe^{-r}$ (dashed lines). The Mode III stress intensity factors $K_-^{(r)}$ (for a delamination crack below a rigid interface) are given here for comparison

condition along the positive semi-axis and the Neumann traction condition on the negative semi-axis. The material parameters used in the computations are the same as those of section 6.2 and are presented in Table 2. In all the cases the interphase layer is made of iron. The curves labelled by '1' correspond to aluminium above and magnesium below the interface, these materials interchange for the curves labelled by '2', and the case '3' corresponds to aluminium placed on both sides of the interface.

In Fig. 13(a) we show the stress intensity factor $K^{(d)}/p$ versus V/v_m. It corresponds to the symmetric load $g_\pm = pre^{-r}$, with p constant (solid lines), and the non-symmetric load $g_+ = pe^{-r}$, $g_- = pre^{-r}$ (dashed lines). We note that the load applied to the lower face of the moving crack is the same in both cases, and this load vanishes as $r \to 0$. Figure 13(b) corresponds to the case of symmetric load with $g_\pm = pe^{-r}$ (solid lines), and non-symmetric load, with $g_+ = pre^{-r}, g_- = pe^{-r}$ (dashed lines). Both cases have the same load on the lower face of the crack, but this load does not vanish as $r \to 0$, in contrast with the case of Fig. 13(a).

The computations presented in the two figures show that the relatively stiff iron interface produces output sufficiently close to the case of a perfectly rigid interface (shown by dashed lines on the diagrams). Also, we remark that the change of the load applied to the upper face of the crack (which is in contact with the stiff interface) produces a small change in the values of $K^{(d)}/p$. The variation of the stress intensity factor with the crack velocity is also negligibly small.

Comparison of Fig. 13(a) and Fig. 13(b) also suggests that $|K^{(d)}/p|$ for the case of Fig. 13(a) (where the load on the lower face of the crack vanishes as $r \to 0$) is larger than $|K_-^{(r)}/p|$, whereas in the other case, shown in Fig. 13(b), $|K^{(d)}/p| < |K_-^{(r)}/p|$.

To summarize, we have obtained analytical results on regularity of solutions to problems of cracks propagating along imperfect interfaces and presented numerical simulations that include accurate

evaluation of displacement and stress around the delamination cracks for a range of realistic physical parameters. It is shown that the classical concepts of fracture mechanics may require adjustments for problems involving delamination on stiff or soft interfaces.

Acknowledgements

This research project has been supported by a Marie Curie Transfer of Knowledge Fellowship of the European Community's Sixth Framework Programme under contract number (MTKD-CT-2004-509809). The paper has been completed during the Marie Curie Fellowship of G. Mishuris at Liverpool University. Provision of academic facilities by the Department of Mathematical Sciences, Liverpool University, is gratefully acknowledged.

References

1. R. Lipton and B. Vernescu, Composites with imperfect interface, *Proc. R. Soc.* A **452** (1996) 329–358.
2. D. Bigoni, S. K. Serkov, M. Valentini and A. B. Movchan, Asymptotic models of dilute and densely packed composites with imperfectly bonded inclusions, *Int. J. Solids Struct.* **35** (1998) 3239–3258.
3. Y. Benveniste and T. Chen, On the Saint-Venant torsion of composite bars with imperfect interfaces, *Proc. R. Soc.* A **457** (2001) 231–255.
4. O. Avila-Pozos and A. B. Movchan, Slow decay of end effects in layered structures with an imperfect interface, *J. Engng Math.* **45** (2003) 155–168.
5. Z. Hashin, Thin interphase/imperfect interface in elasticity with applications to coated fibre composites, *J. Mech. Phys. Solids* **50** (2002) 2509–2537.
6. G. Mishuris, Imperfect transmission conditions for a thin weakly compressible interface, *Arch. Mech.* **56** (2004) 103–115.
7. S. K. Kanaun, Equilibrium of a homogeneous elastic medium that is reinforced by a rectilinear solid rod, *J. Appl. Math. Mech.* **52** (1988) 616–624.
8. E. N. Vilchevskaya and S. K. Kanaun, Integral eqautions for a problem on a thin inclusion in a homogeneous elastic medium, *ibid.* **56** (1992) 235–243.
9. Y. A. Antipov, A. B. Movchan and N. V. Movchan, Frictional contact of a fibre and an elastic solid, *J. Mech. Phys. Solids* **48** (2000) 1413–1439.
10. C. Atkinson, On stress singularities and interfaces in linear elastic fracture mechanics, *Int. J. Fract.* **13** (1977) 807–820.
11. Y. A. Antipov, O. Avila-Pozos, S. T. Kolaczkowski and A. B. Movchan, Mathematical model of delamination cracks on imperfect interfaces, *Int. J. Solids Struct.* **38** (2001) 6665–6697.
12. G. Mishuris and G. Kuhn, Asymptotic behaviour of the elastic solution near the tip of a crack situated at a nonideal interface, *ZAMM* **81** (2001) 811–826.
13. G. Mishuris, Mode III interface crack lying at thin nonhomogeneous anisotropic interface. Asymptotics near the crack tip, *Asymptotics, Singularities and Homogenisation in Problems of Mechanics* (ed. A. B. Movchan; Kluwer, Dordrecht 2002), 221–230.
14. L. B. Freund, *Dynamic Fracture Mechanics* (Cambridge University Press 1998).
15. A. B. Movchan and N. V. Movchan, *Modelling of Elastic Solids with Non-regular Boundaries* (CRC Press, Boca Raton 1995).

16. Y. A. Antipov and V. V. Silvestrov, Vector functional-difference equation in electromagnetic scattering, *IMA J. Appl. Math.* **69** (2004) 27–69.
17. G. S. Mishuris, On a class of singular integral equations, *Demonstratio Mathematica* **28** (1995) 781–794.
18. W. T. Koiter, On the diffusion of load from a stiffener into a sheet, *Q. Jl Mech. Appl. Math.* **8** (1955) 164–178.
19. S. Lenci, Analysis of a crack at a weak interface, *Int. J. Fract.* **108** (2001) 275–290.